Sheet flow dynamics under monochromatic nonbreaking waves

C. Marjolein Dohmen-Janssen
Department of Civil Engineering, University of Twente, Enschede, Netherlands

Daniel M. Hanes
Department of Civil and Coastal Engineering, University of Florida, Gainesville, Florida, USA

Received 3 July 2001; revised 22 April 2002; accepted 17 May 2002; published 16 October 2002.

[1] For the first time, detailed measurements of sediment concentrations and grain velocities inside the sheet flow layer under prototype surface gravity waves have been carried out in combination with measurements of suspension processes above the sheet flow layer. Experiments were performed in a large-scale wave flume using natural sand. Sand transport under high waves in shallow water is mainly contained within the so-called "sheet flow layer," a thin layer (10–60 grain diameters) in which the volume concentration of sand decreases by an order of magnitude from a value near 0.6 at the stationary bed. The thickness of the layer varies over a wave cycle and the maximum thickness increases with increasing peak Shields stress. The concentrations within the sheet flow layer vary approximately synchronously with the orbital velocity measured by an Acoustic Doppler Velocimeter (ADV) located 0.1 m above the bed, with typical phase lags of $0-\pi/5$. In contrast, the suspended sediment concentrations a few centimeters and higher above the bed exhibit larger phase lags. Grain velocities were successfully measured in the middle and upper portions of the sheet flow layer around the time of their maximums. These velocities increased weakly with elevation from approximately 50% to 70% of the velocity outside the wave boundary layer. The observations are compared to previous experimental work and are found to be mainly consistent with observations in steady unidirectional flows and in oscillating water tunnels (OWTs), although differences in the suspended sediment concentration and the total sediment transport rate are apparent. Observations are also compared to two very different models: a 1DV suspension model for oscillatory flow with enhanced boundary roughness and a two-phase collisional grain flow model for steady unidirectional flow. While the suspension model describes the velocity profile fairly well and the collisional model describes the concentration profile well, neither model accurately predicts both the velocity and the concentration and therefore the sediment flux over the full vertical extent of the sheet flow. *INDEX TERMS:* 4546 Oceanography: Physical: Nearshore processes; 4558 Oceanography: Physical: Sediment transport; 3022 Marine Geology and Geophysics: Marine sediments—processes and transport; 3020 Marine Geology and Geophysics: Littoral processes; *KEYWORDS:* sediment transport; sheet flow; bed load; suspension; large wave flume; sand transport models

Citation: Dohmen-Janssen, C. M., and D. M. Hanes, Sheet flow dynamics under monochromatic nonbreaking waves, *J. Geophys. Res.*, *107*(C10), 3149, doi:10.1029/2001JC001045, 2002.

1. Introduction

[2] Nearshore morphological evolution is strongly determined by the complex mechanisms of sediment transport caused by the action of waves and currents. Sheet flow is an important transport regime because it occurs during storm conditions when large quantities of sand are transported. Due to the large bed shear stresses under these conditions, ripples are washed out, the bed becomes relatively flat, and the sand is mainly transported in a thin layer with high sediment concentrations close to the bed, i.e., the sheet flow layer.

0148-0227/02/2001JC001045$09.00

[3] In order to improve sediment transport modeling, information is needed about near-bed sediment transport processes. Field observations have yielded a lot of information on suspension processes above rippled and plane beds. The influences of wave conditions, wave groups, sediment size, sediment gradation, etc., have been studied for example by *Vincent and Green* [1990], *Hanes* [1991], *Kroon* [1994], *Hoekstra et al.* [1994], *Houwman and Ruessink* [1996], *Lee and Hanes* [1996], *Van Rijn* [1998], *Hanes et al.* [1998], and *Jimenez et al.* [1998]. However, in the field it remains very difficult to perform detailed measurements within the dense mobile sediment layer close to the seabed. Therefore, many experiments on sand transport in sheet flow conditions have been carried out in laboratories, mainly in oscillating water tunnels (hereafter OWTs), e.g.,

the works of *Horikawa et al.* [1982], *Sawamoto and Yamashita* [1986], *Asano* [1992], *Dibajnia and Watanabe* [1992], and *Li and Sawamoto* [1995]. Large OWTs with prototype values of near-bed oscillatory velocities (up to 2 m/s) and oscillation periods (5–12 s) were used by *King* [1991], *Ribberink and Al-Salem* [1994, 1995], *Ribberink* [1998], *Zala Flores and Sleath* [1998], *McLean et al.* [2001], and *Dohmen-Janssen et al.* [2002].

[4] *Horikawa et al.* [1982] were among the first to measure details of oscillatory sheet flow, like the inception of sheet flow, the thickness of the sheet flow layer, time-dependent concentrations profiles inside the sheet flow layer and resulting sediment transport rates for 0.2 mm sand. They found that most of the transport takes places inside the sheet flow layer, which has a thickness in the order of 10 mm. These observations were confirmed by the full-scale OWT experiments of *Ribberink and Al-Salem* [1994] with asymmetric (second-order Stokes) oscillatory sheet flows and similar sand (0.21 mm). Ribberink and Al-Salem concluded that sediment transport in oscillatory sheet flow behaves approximately quasi-steady. Indeed, a quasi-steady model was found to yield good predictions of the net transport rates for most oscillatory and combined wave–current sheet flow conditions [*Ribberink*, 1998].

[5] Time-dependent measurements of sediment concentrations [*Ribberink and Al-Salem*, 1995] showed that the sheet flow layer consists of two layers: a pick-up layer located below the initial bed level and an upper sheet flow layer located above it. Moreover, concentrations within the sheet flow layer were found to be nearly in phase with the near-bed velocities, while suspended sediment concentrations showed much larger phase lags. However, *Horikawa et al.* [1982] found indications that differences between the accelerating and decelerating phase led to differences in concentration profiles inside the sheet flow layer, indicating that the transport process in the sheet flow layer does not just depend on the velocity (which was the same because of the sinusoidal motion). Moreover, *Dibajnia and Watanabe* [1992] carried out experiments with short wave periods and found that in many cases a quasi-steady transport model failed to describe the magnitude and the direction of the net transport rate. They expected phase lags between velocity and concentration to be responsible. *Dohmen-Janssen et al.* [2002] extended the full-scale data set of net transport rates and time-dependent velocities and concentrations to sheet flow conditions of sinusoidal oscillatory flow combined with a net current for sand with different grain sizes (i.e., 0.13, 0.21, and 0.32 mm). They found that for fine sand phase lags between the near-bed velocity and the concentrations inside the sheet flow layer may become so large that they lead to reduced net transport rates [*Dohmen-Janssen et al.*, 2002].

[6] *McLean et al.* [2001] measured grain velocities within the sheet flow layer under similar conditions as *Dohmen-Janssen et al.* [2001] for fine (0.13 mm) and coarse sand (0.32 mm). They found relatively large velocities close to the undisturbed bed which lead to large sediment fluxes because of the high sediment concentrations in this region. This confirmed the earlier observations that most of the sediment transport takes place within the sheet flow layer.

[7] Because most of the transport occurs within the sheet flow layer, the thickness of this layer is an important parameter. The sheet flow layer thickness is closely related to the erosion depth. Many researchers [e.g., *Wilson*, 1989; *Sawamoto and Yamashita*, 1986; *Asano*, 1992; *Sumer et al.*, 1996] have observed an approximately linear relation between the nondimensional sheet flow layer thickness or the nondimensional erosion depth (normalized by the grain diameter of the sediment) and the Shields parameter, qualitatively as predicted on theoretical grounds by *Bagnold* [1956]. However, *Li and Sawamoto* [1995] found that the sheet flow layer thickness also depends on the unsteadiness of the flow. Similarly, *Zala Flores and Sleath* [1998] found that the erosion depth depends both on the Shields parameter and on the ratio of inertial to gravity force. *Inman et al.* [1986] performed measurements in the field and observed that for fine sand (D_{50} = 0.15 mm) bursting occurred near the moment of maximum velocity, resulting in a significant increase in the thickness of the sheet flow layer. *King* [1991] measured similar phenomena for fine sand (D_{50} = 0.135 mm) in a large OWT. He expected that bursting was restricted to fine grain sediments. *Dohmen-Janssen et al.* [2001] also found that in oscillatory flow the sheet flow layer thickness for fine sand (D_{50} = 0.13 mm) is significantly larger than for coarser sand ($D_{50} \geq 0.21$ mm).

[8] The different observations regarding fine sand verses coarse sand sheet flow dynamics were partially explained by *Sumer et al.* [1996]. They showed that depending upon the ratio of the particle fall velocity to the friction velocity at the bed, the immersed weight of the particles in the sheet flow may either be supported by intergranular collisions or alternatively by the turbulent fluctuations in the fluid velocity. These alternate mechanisms may also be active to different degrees in a unidirectional sheet flow (even with fixed particle and fluid properties), depending upon the vertical location within the sheet. In oscillatory sheet flows we would expect the relative importance of these processes to depend both upon vertical location and also upon time (or wave phase), because the shear stress passes through zero during the oscillation.

[9] Observations in OWTs have increased insight into oscillatory sheet flow processes. However, it is likely that transport processes under propagating waves are somewhat different from those in horizontal uniform oscillatory flows. Although OWTs are capable of simulating orbital velocities, some differences remain:

1. OWT flow is uniform in the flow direction, while the orbital motion under waves has gradients in the direction of wave propagation.
2. The ensemble (phase)-averaged flow in OWTs is purely horizontal, while the orbital motion under waves contains a vertical component. Consequently, an onshore-directed boundary layer streaming is present under waves, which is absent in OWTs.
3. Vertical turbulent fluctuations are probably suppressed in OWTs because of the influence of a rigid lid, so the distribution of Reynolds stress may be different.
4. Both in an OWT and under propagating waves the horizontal pressure gradient is in phase with the flow acceleration. However, because of the uniform flow in OWTs, the pressure itself is in phase with its gradient and is thus in phase with the acceleration, while under waves the pressure is 90° out of phase with its gradient and is thus in phase with the velocity rather than with the acceleration.

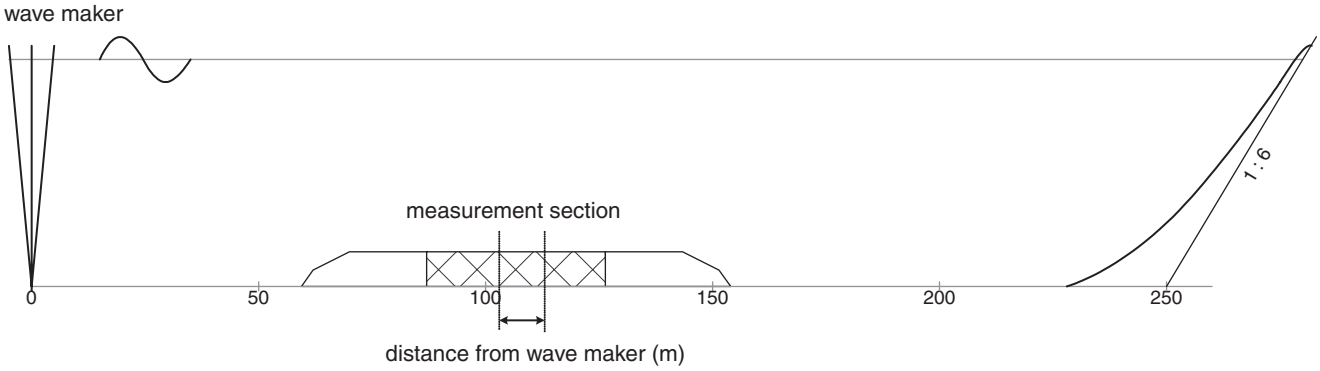

Figure 1. Outline of the wave flume with the test section.

[10] It is expected that the flow very close to the bed and thus sheet flow processes are rather well simulated in OWTs, because close to the bed the vertical component of the orbital velocity is small and the vertical velocity gradients are much larger than the horizontal velocity gradients. However, since almost all knowledge about sheet flow processes is obtained from OWT experiments it is important to investigate whether this is true. Further away from the bed, in the suspension layer, differences between transport processes under waves and in uniform oscillatory flows may be much larger. In order to increase insight in suspension processes it is important to study them in relation to the near-bed transport processes. Therefore, new experiments were carried out in the Large Wave Flume in Hannover, Germany, in which detailed measurements of net transport rates, bed form characteristics and near-bed flow velocities and sediment concentrations were performed under various prototype wave conditions, both in the rippled bed and in the sheet flow regime. All measurements were carried out above a horizontal bed of well-sorted sand (D_{50} = 240 μm).

[11] The aim of this paper is to describe our observations of sheet flow sediment transport under monochromatic wave conditions and compare them to theories and previous observations of similar phenomena. For the first time, detailed measurements of sediment concentrations and grain velocities inside the sheet flow layer under prototype surface gravity waves were combined with measurements of suspension processes above the sheet flow layer. From these measurements the thickness of the sheet flow layer has been determined as well as the sediment flux in the suspension layer and in the sheet flow layer. In addition, total net transport rates have been determined from bed profile measurements. The basis for the present sheet flow experiments were the large-scale OWT experiments of *Ribberink and Al-Salem* [1994, 1995] with asymmetric oscillatory flow and no net current, because these experiments closely resemble the situation in a large-scale shallow water wave flume with nonbreaking waves.

2. Experimental Set-Up

2.1. Large Wave Flume With Test Section and Instruments

[12] The experiments were performed in the Large Wave Flume (Großer WellenKanal, GWK) of the ForschungsZentrum Küste in Hannover, Germany. The flume has a length of 300 m, a width of 5 m and a depth of 7 m and has a wave paddle on one end and a 1:6 dike on the other end. The wave paddle can generate regular as well as irregular waves over a range of wave heights (±0.5–2 m) and wave periods (±2–15 s) corresponding to prototype values. The wave maker is equipped with a reflection compensation. Usual water depths in the flume vary between 4 and 5 m.

[13] A test section, consisting of a 45 m long, 5 m wide and 0.75 m thick horizontal sand bed was positioned between x = 85 m and x = 130 m (x = 0 at the wave paddle). The sand bed was formed by well-sorted quartz (ρ_s = 2650 kg/m^3) with a median grain diameter of about 240 μm (D_{10} = 173 μm, D_{90} = 277 μm). This sand is similar to sand used in the OWT experiments of *Ribberink and Al-Salem* [1994, 1995], which had the following characteristics: D_{10} = 150 μm, D_{50} = 210 μm, D_{90} = 320 μm. Raised horizontal bottoms with the same height as the sand bottom and covered with asphalt were constructed at both ends of the sand bed over a length of about 15 m. A beach profile of coarser sand (D_{50} = 0.3 mm) and a slope of about 1:10 was placed against the 1:6 dike for energy dissipation. Figure 1 shows a schematic diagram of the flume with the test section.

[14] Different instrument frames were installed in the central part of the test section. For an overview of the complete instrumental set-up the reader is referred to the work of *Ribberink et al.* [2000]. The measured parameters and measuring techniques that we focus on in this paper are presented in the next section.

2.2. Measured Parameters and Measuring Techniques

2.2.1. Net Transport Rates

[15] Net transport rates along the test section were determined by application of the continuity equation, using successive profile surveys. The continuity equation approach maintains that the difference between sediment flowing into a given region (q_{sin}) and the sediment flowing out of the region (q_{sout}) must be accounted for by a change in the bed elevation of that region per unit time (dV/dt):

$$q_{sin} - q_{sout} = (1 - \varepsilon_0)\frac{dV}{dt} \quad (1)$$

[16] Here, ε_0 is the porosity of the sand bed. Values of the porosity may vary. For example the porosity of sand that has

just been deposited may be higher than the porosity of a sand bed that has been subject to wave action. Previous experiments with similar sand in an OWT showed values of ε_0 varying between 0.33 and 0.47, with an average value of 0.38 [*Van der Hout*, 1997]. The exact value ε_0 in the present tests is not known. We therefore assume a constant value of $\varepsilon_0 = 0.4$, which is sufficiently accurate given the accuracy of the bed level measurements. In order to determine dV/dt, the bed level before and after each test was measured using a Multiple Transducer Array (MTA, see below). In order to solve equation (1), at least one boundary condition must be known. During the experiments it turned out that no sand was transported against the direction of wave propagation. Therefore net transport rates at the paddle-side boundary of the test section were set to zero.

2.2.2. Bed Levels

[17] An MTA similar to the one described by *Hanes et al.* [2001] was used to survey the sand bed profile along the entire centerline of the test area. The present MTA consists of 32 five-MHz transducers separated by 2 cm each. Each transducer is pinged in succession, and each acts as a threshold detecting sonar device. The MTA was mounted on a frame that was attached to the measuring carriage, which moved along the tank to measure the bed profile in between two experimental runs. Before each profile measurement, the frame was lowered to a fixed level, such that the MTA was positioned horizontally about 0.5 m above the sand bed. The MTA was oriented 45° with respect to the centerline of the flume in order to measure bed level variations in a 45 cm wide strip across the flume.

[18] The horizontal resolution is determined by the sampling frequency of the MTA (1.7 Hz) and the velocity of the carriage (6.5 m/min). This yields a horizontal resolution of about 65 mm. Due to the orientation of the MTA, averaging the results of the different transducers (i.e., across the flume) yields a horizontal resolution of about 3 mm. The vertical resolution of the MTA is determined by its ability to measure the elapsed time between the transmission of a sound pulse and the detection of the exceedance of a threshold return. This results in a *resolution* of less than 1 mm. However, the (vertical) *accuracy* of the MTA is influenced by a variety of environmental conditions and is estimated to be approximately 2 mm for this experiment.

2.2.3. Local Measurements of Flow Velocity and Sediment Concentration

[19] Attached to a vertical pole on the measuring carriage (on the opposite side of the profile frame) were an Acoustic Doppler Velocimeter (ADV) [see *Lohrmann et al.*, 1994] and a Transverse Suction System (TSS) (similar to the one developed by *Bosman et al.* [1987]). During the measurement they were positioned at x = 109.2 m. The ADV was used to measure alternately three components of the near-bed flow velocity and the level of the sand bed underneath the probe. The sampling volume of the ADV is located about 5.9 cm below the probe tip and has a (horizontal) diameter of about 6 mm and a thickness of about 9 mm. The TSS was used to measure time-averaged (i.e., averaged over 5–10 min or about 30–100 waves) suspended sediment concentration and grain size distribution profiles by extracting samples of suspended sediment in a direction normal to the flow at ten different levels simultaneously. The intake nozzles (inner ϕ 3 mm, outer ϕ 5 mm) stick out 50 mm from the vertical pole. Close to the ADV, a Conductivity Concentration Meter system (CCM system) was buried under the sand bed to measure sediment concentrations and grain velocities inside the sheet flow layer. Measured concentration profiles were used to determine the sheet flow layer thickness. Figure 2 shows a schematic diagram of this set-up.

[20] The CCM system was specifically developed for the present flume tests. It consists of two CCMs (developed by Delft Hydraulics, see, e.g., *Ribberink and Al-Salem* [1995]), installed in a waterproof enclosure that was buried under the sand bed, such that the CCM probes penetrated the sheet flow layer from below. The probes could be moved up and down using a remotely controlled vertical positioning system. The CCM system was installed in the flume such that the two CCM probes were aligned in along-flume direction. With each probe, concentrations are only measured at a single point at the time. Therefore, repetitive tests have been carried out with the CCMs positioned at different elevations relative to the bed, in order to cover the entire sheet flow layer in the measurements.

[21] The CCM is designed to measure high sand concentrations ($\approx$100–2000 g/l or 0.04 to 0.75 by volume). It consists of four electrodes (thickness 0.3 mm, distance between them 0.6 mm) and measures the electrical conductivity of the sand/water mixture, which is related to the volume concentration of sand. The vertical thickness of the sensing volume is approximately 1–1.5 mm. In the present experiments two CCM probes were used at the same vertical elevation but separated by 15 mm in the horizontal (flow) direction in order to determine grain velocities by cross-correlation of the two concentration signals.

[22] Acoustic backscatter sensors (ABS) [see *Thorne and Hanes*, 2002] were used to measure the suspended sediment concentration profile as a function of time and elevation above the seabed. These sensors provided estimates of concentration with 0.75 cm vertical resolution and 0.25 s temporal resolution. They were mounted on a frame that was attached to the sidewall of the flume (at x = 106 m). The instruments were positioned about 1 m from the sidewall. This frame also held two additional ADVs to measure the local near-bed flow velocity, an MTA to measure the local small-scale bed form dimensions and a pressure sensor to measure wave height.

2.3. Test Conditions

[23] Hydraulic conditions varied from monochromatic waves to wave groups, random waves and bimodal random waves, both in the rippled bed and in the sheet flow regime. In this paper we focus on the tests with monochromatic sheet flow conditions. The monochromatic waves generated by the wave maker are very similar in shape to cnoidal waves.

[24] Test conditions are presented in Table 1. This table includes the design wave height at the wave maker H_{des}, the wave period T, the height of the sampling volume of the ADV above the sand bed z_{adv}, the horizontal velocity measured at that level and the number of half-hour runs per test condition, N. For each condition, the measured velocity is represented by the average values over the different half-hour runs of the root mean square velocity u_{rms}, the mean velocity u_m and the velocities under the crest and the trough of the wave, u_c and u_t. For all tests, the water

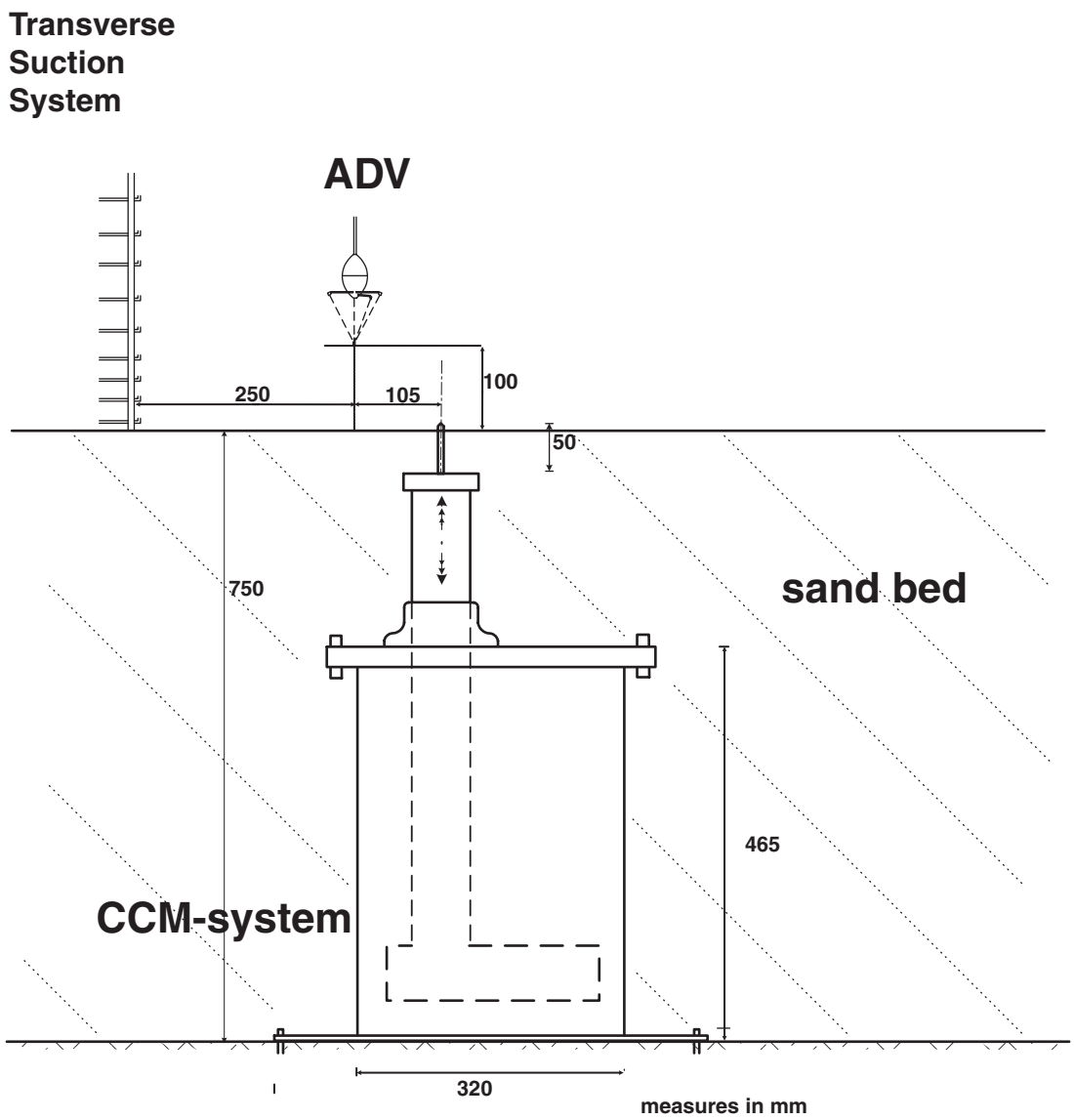

Figure 2. Schematic diagram of the set-up of local measurement frame with ADV, TSS, and CCMs.

depth at the wave paddle was 4.25 m, corresponding to a water depth above the sand bed of 3.5 m.

[25] Table 1 also presents a value of the Shields parameter under the crest and the trough of the wave, θ_c and θ_t. This value of θ is calculated using a wave friction factor according to *Swart* [1974] and a mobile-bed roughness height given by the expression of *Sumer et al.* [1996] to take into account the fact that the roughness height in sheet flow is larger than the grain size. Notice that Sumer et al.'s expression for mobile-bed roughness height was derived for steady flow. Because we expect sheet flow under waves to behave more or less quasi-steady, we think that using this steady flow mobile-bed roughness relation gives a reasonable approximation for the values of the Shields parameter under the crest and the trough of the wave. According to this expression, the roughness is a function of the Shields parameter and the ratio of settling

Table 1. Overview of Monochromatic Sheet Flow Conditions

Test condition	H_{des} (m)	T (s)	z_{adv} (mm)	u_{rms} (m/s)	u_m (m/s)	u_c (m/s)	u_t (m/s)	θ_c (−)	θ_t (−)	N (−)
mk	1.2	6.5	90	0.57	−0.041	0.92	−0.76	1.08	0.77	1
mi	1.35	6.5	103	0.59	−0.045	0.98	−0.79	1.21	0.83	4
ml	1.5	6.5	103	0.66	−0.057	1.11	−0.87	1.53	0.99	1
mh	1.6	6.5	109	0.62	−0.037	1.09	−0.72	1.42	0.71	4
mn	1.2	9.1	109	0.65	−0.035	1.26	−0.70	1.76	0.61	1
mf	1.3	9.1	99	0.66	−0.037	1.31	−0.70	1.89	0.61	6
mm	1.4	9.1	107	0.74	−0.055	1.54	−0.67	2.58	0.57	1
me	1.5	9.1	99	0.68	−0.052	1.45	−0.64	2.30	0.52	6

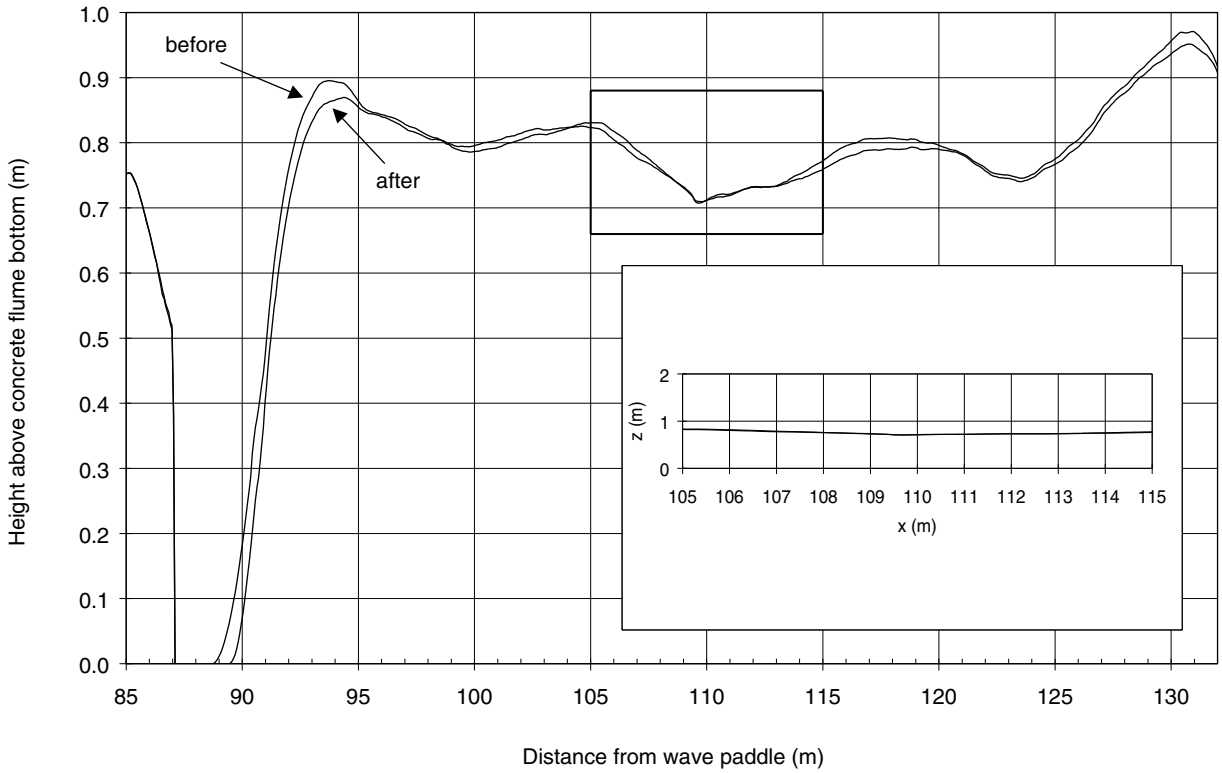

Figure 3. Example of measured bed profiles before and after an experimental run (mee). The inset shows the bed profile around the measurement location (x = 109 m) at undistorted scale.

velocity to friction velocity. The expression for the wave friction factor of Swart is an explicit approximation to the implicit formulation of *Jonsson* [1966], which is valid for rough turbulent flow over fixed beds. Values of the Reynolds number ($Re = u \times a/\nu$) and the relative roughness (a/k_s) for the present experiments, calculated using the *Sumer et al.* [1996] expression for the roughness, were found to lie in the range of 5×10^5 to 3.5×10^6 and 670–1540, respectively, indicating that the flow is probably in the rough turbulent regime. However, if the grain size were used for the roughness then the flow would be in the transitional regime, so there is still some uncertainty regarding the level of turbulence within the sheet.

3. Net Transport Rates

3.1. Bed Profiles and Net Transport Rates Along the Test Section

[26] Figure 3 shows a typical example of two profiles of the sand bed along the test section before and after an experimental run. The profile shows the slope that forms the transition between the asphalt bottom and the test section (x = 85–87 m). At this stage in the experiments, an erosion hole has been developed on the "offshore" edge of the test section. At the beginning of this specific run the erosion hole has reached the bottom of the flume (z = 0) between x = 87 m and x = 89 m. By the end of the run, the erosion hole has grown: apparently sand has been transported in the shoreward direction during this run. The erosion hole, when it existed, never reached the measurement position, located at x = 106–109 m. Because of the distorted scale (1 m vertically, 55 m horizontally) in Figure 3, some long-scale bed features can be observed. However, they have very mild slopes (0.03 in this case), which can be seen in the inset that shows the two bed profiles around the measurement location (x = 105–115 m) at undistorted scale.

[27] Figure 4 shows the net transport rate along the offshore part of the test section (x = 85–115 m), calculated from the difference in bed level between the two profiles shown in Figure 3. No sand is present for x < 89 m (asphalt bottom and erosion hole). Consequently, the net transport rate is zero here. For x > 89 m, the net transport rate sharply increases, until the "transport capacity" is reached and the net transport rate becomes more or less constant (x = 95–115 m). The net transport rate for this run is determined as the average net transport rate over a 2.5 m long region around x = 109 m (the location where the velocity is measured, indicated by the dashed line). The same procedure is followed for all the tests for which net transport rates were measured (conditions me, mf, mh, and mi) and the results of the different runs are averaged for each wave condition.

3.2. Net Transport Rates Under Waves and in Uniform Horizontal Oscillatory Flows

[28] Figure 5 presents the net transport rate $\langle q_s \rangle$ against the time-averaged third power of the cross-shore fluid velocity $\langle u^3 \rangle$, where u is the ensemble average of the measured fluid speed at approximately 0.1 m above the still sand bed. The solid circles show the average results over several runs with the same wave conditions of the present flume tests. The error bars indicate the standard

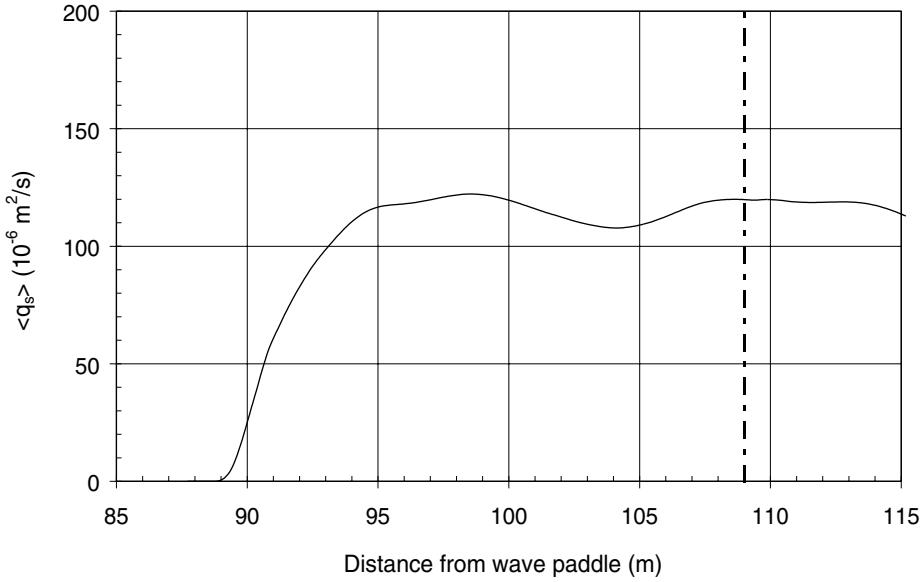

Figure 4. Example of measured net transport rates for one experimental run (mee), from the beginning of the test section to the measurement location (x = 109 m).

deviation in $\langle q_s \rangle$ and $\langle u^3 \rangle$ over the different runs. Values of $\langle u^3 \rangle$, $\langle q_s \rangle$, and their standard deviations can be found in Table 2. In addition, Figure 5 presents results obtained form measurements in a large OWT [*Ribberink and Al-Salem*, 1994]. Lines are fitted (forced through zero) through both data sets.

[29] Figure 5 shows that a linear relation between the net transport rates and the third-power velocity moment is a reasonable assumption in both cases. However, net transport rates under waves are about a factor 2.5 larger than in uniform horizontal oscillatory flows, probably because of the previously mentioned differences between boundary layer flows in OWTs and boundary layer flows under free-surface gravity waves. Model calculations by *Bosboom and Klopman* [2000] indicate indeed that this difference may (partly) be attributed to the onshore-directed boundary layer streaming that is present under waves and is absent in horizontal oscillatory flow. As a rough indication of the effect of a boundary layer streaming on the net transport rate, it is investigated what the effect is of a small positive (onshore) net current on the third-power velocity moment, which is directly related to the net transport rate. Adding a net current with a velocity of 5% of the maximum (crest) velocity to the second-order Stokes velocities of the OWT experiments leads to third-power velocity moments that are a factor 1.4–1.9 larger than without this small net current. This

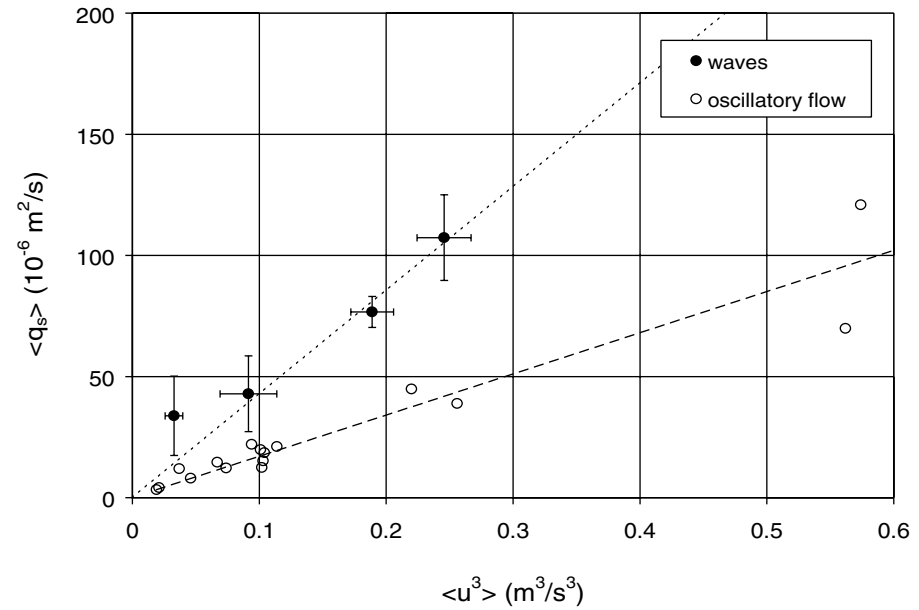

Figure 5. Net transport rate as a function of the third-power velocity moment. Measurements under waves and in horizontal uniform oscillatory flow.

Table 2. Measured Third-Power Velocity Moments, Net Transport Rates, and Their Standard Deviations

Test condition	H_{des} (m)	T (s)	$\langle u^3 \rangle$ (m^3/s^3)	σ_{u3} (m^3/s^3)	$\sigma_{u3}/\langle u^3 \rangle$ (%)	$\langle qs \rangle$ (m^2/s)	σ_{qs} (m^2/s)	$\sigma_{qs}/\langle qs \rangle$ (%)
mi	1.35	6.5	0.033	0.007	21.1	33.8	16.4	48.4
mh	1.6	6.5	0.091	0.022	24.5	42.9	15.6	36.5
mf	1.3	9.1	0.189	0.017	8.9	76.7	6.4	8.4
me	1.5	9.1	0.246	0.021	8.7	107.3	17.7	16.5

factor is the same order of magnitude as the ratio between the measured net transport rates under waves and in uniform oscillatory flow (2.5), which indicates that a small onshore boundary layer streaming may be (partly) responsible for the relatively large increase in net transport rate.

4. Time-Averaged Sediment Concentration Profiles

[30] Figure 6 shows the time-averaged sediment concentration profile for condition mh (T = 6.5 s, H = 1.6 m) on semilogarithmic scale in the lower 0.2 m above the bed. Measurements in the sheet flow layer are from the CCM. In the suspension layer, the figure shows concentrations measured by the TSS and by two ABSs: ABS1 (1 MHz) and ABS2 (2 MHz). The difference between the two ABS estimates is probably due to sediment size effects upon instrument calibration, which have not been considered here. These profiles exhibit strong gradients near the bed, with the vast majority of the moving sediment being contained in a very thin layer. The relatively small vertical gradient in the measured suspended sediment concentrations above 3 cm is somewhat perplexing. It might be due to the presence of fine sediments, or there may be a background level of turbulence that builds up above the wave boundary layer.

[31] The level z = 0 is defined as the level of the initial still bed. This level is determined by shifting the z = 0 level until the amount of sand that is "missing" below z = 0, is equal to the amount of sand entrained into the flow, i.e., the total load. This can be seen more clearly in Figure 7, which shows the time-averaged concentration profile in the lowest 12 mm. The area below z = 0, above the measured concentration profile and to the left of the thin vertical dashed line (representing the still bed concentration) represents the amount of sand "missing" from the bed. This area is equal to the integration of the concentration profile above z = 0, i.e., the total load.

[32] Figure 7 also shows the time-averaged concentrations inside the sheet flow layer of all individual waves (dots in the figure). This gives an indication of the uncertainty in elevation of the CCM measurements, which is about 2 mm (±1 mm). All measured concentrations are grouped in bins, based on their wave-averaged value. The average bin concentrations are plotted against the average bin levels (solid circles in the figure), together with their standard deviations (error bars). These bin averages were plotted in Figure 6.

[33] Figures 6 and 7 show that a very sharp vertical concentration gradient is present close to the bed, with concentrations decreasing from 0.67 m^3/m^3 at approximately 4 mm below the initial bed level to a value of about

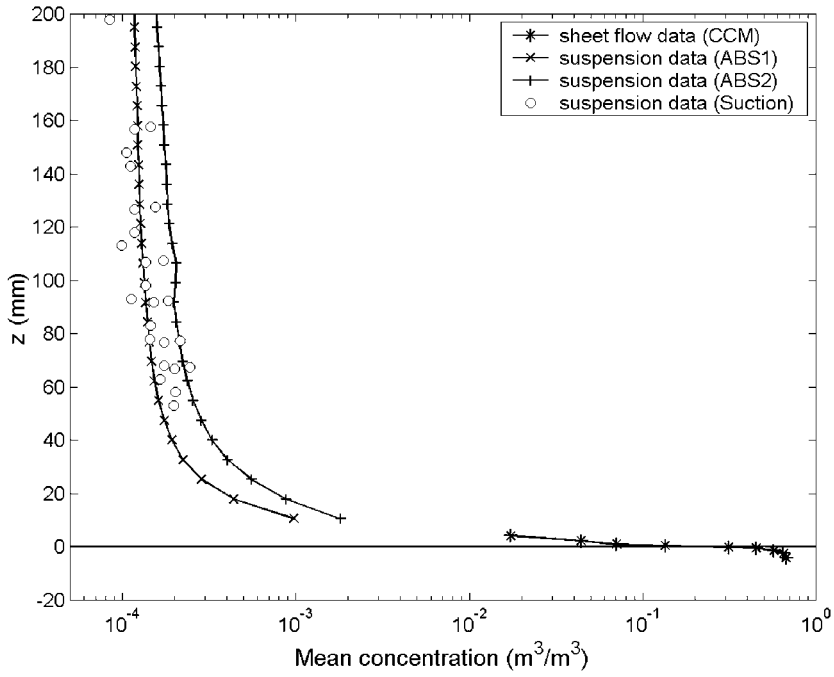

Figure 6. Time-averaged concentration profiles for condition mh.

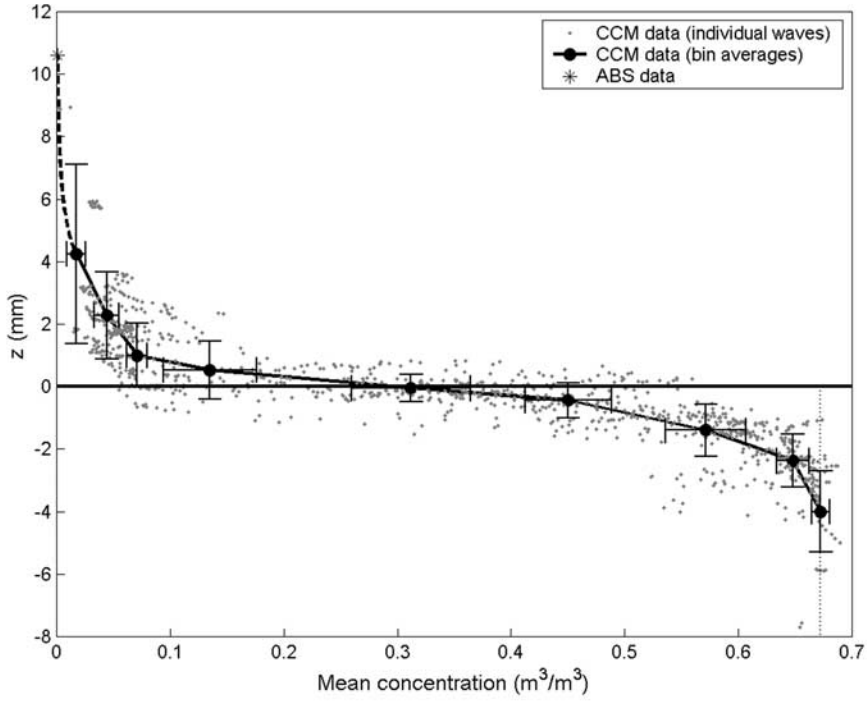

Figure 7. Measured concentrations and the time-averaged concentration profile in the sheet flow layer for condition mh.

0.08 m^3/m^3 at approximately 1 mm above the initial bed level. Concentrations in the suspension layer are orders of magnitude smaller than in the sheet flow layer, and the gradient of the concentration is also significantly smaller in the suspension layer.

[34] *Suspension Layer: Comparison with Large-Scale OWT Data:* Figure 8 shows time-averaged suspended sediment concentration profiles, measured by Transverse Suction, for two conditions with a constant wave period (T = 6.5 s) and two different wave heights (i.e., mh and mi). (The two lines represent measured concentration profiles in uniform oscillatory flow, which will be discussed below). The concentrations are shown on log–log scale. For each condition the measurements of four runs are presented. As one would expect for sheet flow conditions, concentrations are higher for higher waves (and corresponding higher near-bed orbital velocities).

[35] *Smith* [1977] derived an expression for the time-averaged suspended sediment concentrations under waves above a plane bed (similar to the Rouse profile for steady flow), by assuming a diffusion model with a linearly increasing sediment mixing coefficient ($\varepsilon_{sz} = \kappa u_* z$ with κ the Von Karman constant and u_* the friction velocity). This results in a power law distribution of the time-averaged concentration (a straight line on log–log scale):

$$c_m(z) = c_a\left(\frac{z_a}{z}\right)^{\alpha} \qquad \text{with} \qquad \alpha = \frac{w_s}{\kappa u_*} = \frac{w_s z}{\varepsilon_{sz}} \tag{2}$$

With:

$c_m(z)$ time-averaged sediment concentration at level z
c_a reference concentration at the reference level z_a
α concentration decay parameter
w_s settling velocity of the sediment

[36] For 210 μm sand in uniform horizontal oscillatory flow, *Ribberink and Al-Salem* [1994] found a constant value of the concentration decay parameter, equal to about 2.1 over a range of conditions (T = 6.5–9.1 s, u_{rms} = 0.3–0.9 m/s). Moreover, they derived a simple empirical expression to calculate the reference concentration c_a at a reference level z_a of 0.01 m above the bed, which reads:

$$c_a = A u_{rms}^n \tag{3}$$

[37] Values of n and A were found to be equal to n = 2.4 and A = 11.3 g/l × $(s/m)^{2.4}$. This equation is dimensional and may depend for example on the grain size. Still, it is applied here in order to get an estimate of the concentration profile in oscillatory flow (using equation (2) with α = 2.1) and compare that with the measurements under waves. This is assumed to be valid because the flow conditions and the sediment in the flume experiments are similar to those in the OWT (i.e., T = 6.5 s, u_{rms} = 0.6 m/s, D_{50} = 240 μm). These estimated concentration profiles in oscillatory flow are represented by the two lines in Figure 8. Comparing the measured concentration profiles in oscillatory flow (lines) with the measured concentration profiles under waves (symbols) shows that under waves the decrease in suspended sediment concentration with height is much smaller than in oscillatory flow. The value of the concentration decay parameter α is about 0.55 for the two concentration profiles under waves (values of α are found by fitting a power law through the data). Consequently, further away from the bed

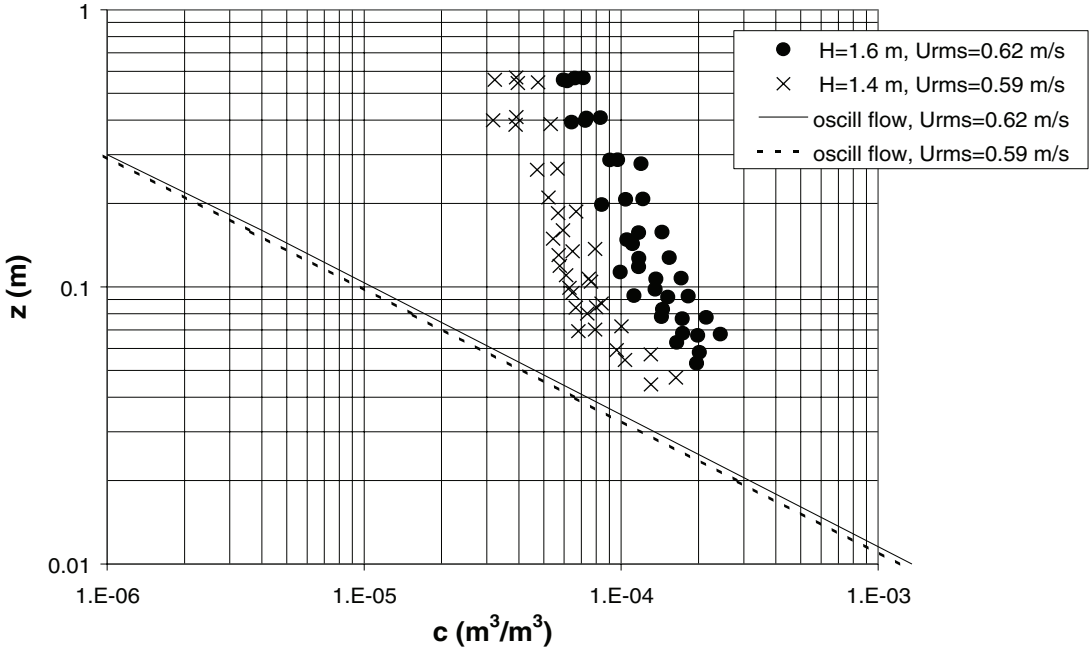

Figure 8. Comparison between measured time-averaged suspended sediment concentrations under waves (from TSS; conditions mh and mi) and an empirical relation, derived from measurements in horizontal uniform oscillatory flow.

the suspended sediment concentrations under waves are far higher than in oscillatory flow, with differences of more than a factor 10 for levels higher than 0.2 m above the bed. Still, close to the bed the differences are smaller and seem to disappear at lower levels. The latter would be expected because near-bed processes are supposed to be simulated rather well in an OWT, while further away from the bed differences may be larger, for example due to the suppression of a vertical velocity component in an OWT due to the rigid upper lid.

[38] The measured increase in concentration in run mi relative to run mh due to the increase in near-bed orbital velocity is larger than predicted by the empirical expression. The root mean square velocity between the two runs increases by about a factor of 1.05, which leads to a predicted increase in concentration with a factor of about 1.12 ($1.05^{2.4}$). However, the measured concentrations increase by about a factor 2. Note that the increase in crest velocity (a factor of 1.12 between these two conditions) is larger than the increase in root mean square velocity. For the conditions of *Ribberink and Al-Salem* [1994] the increase in crest velocity was the same as the increase in root mean square velocity. If the time-averaged concentration profile is strongly determined by the maximum velocity, this might (partially) explain the difference between the predicted and the measured increase in concentration.

5. Time-Dependent Sediment Concentrations

5.1. Ensemble-Averaged Concentration Time Series

[39] Measured concentration time series exhibit large random fluctuations due to the chaotic interactions between individual sediment grains in the sheet flow layer, and between suspended sediment and fluid turbulence in the suspension region. For this reason measured concentrations are ensemble-averaged according to wave phase over many waves to provide time series. Figure 9 shows the ensemble-averaged concentrations in the suspension layer measured by ABS (lower panel) and in the sheet flow layer (middle panel), together with the ensemble-averaged near-bed velocity, measured by the ADV at about 0.1 m above the bed (upper panel). The numbers in the middle panel give the average bin elevation and the number of waves that have been ensemble-averaged (between parentheses).

[40] At the deepest level ($z = -4$ mm) the concentration remains constant throughout the wave cycle at a value of about 0.67 m^3/m^3 (still bed value), indicating that no sand is moving at this level. Between $z = -4$ mm and $z = 0$ mm is the pick-up layer: at $z = -2.4$ mm, the concentration under the crest of the wave decreases, because sediment is being picked up from the bed by the near-bed velocity. At higher elevations ($z = -1.4$ mm and $z = -0.4$ mm), sand is also being picked up under the trough of the wave. However, the decrease in concentration is smaller than under the crest of the wave due to the lower near-bed velocity under the trough than under the crest of the wave.

[41] The upper sheet flow layer is located just above the initial bed level. In the upper sheet flow layer the concentration is coherent with the velocity, because sediment is entrained from the pick-up layer. The concentrations under the trough of the wave are lower and decrease faster with height than under the crest of the wave. This is again caused by the strongly asymmetric near-bed velocities. Between the pick-up layer and the upper sheet flow layer, near the level of the initial still bed ($z = 0$), the measured concentration is more or less constant around 0.3 m^3/m^3. However, this

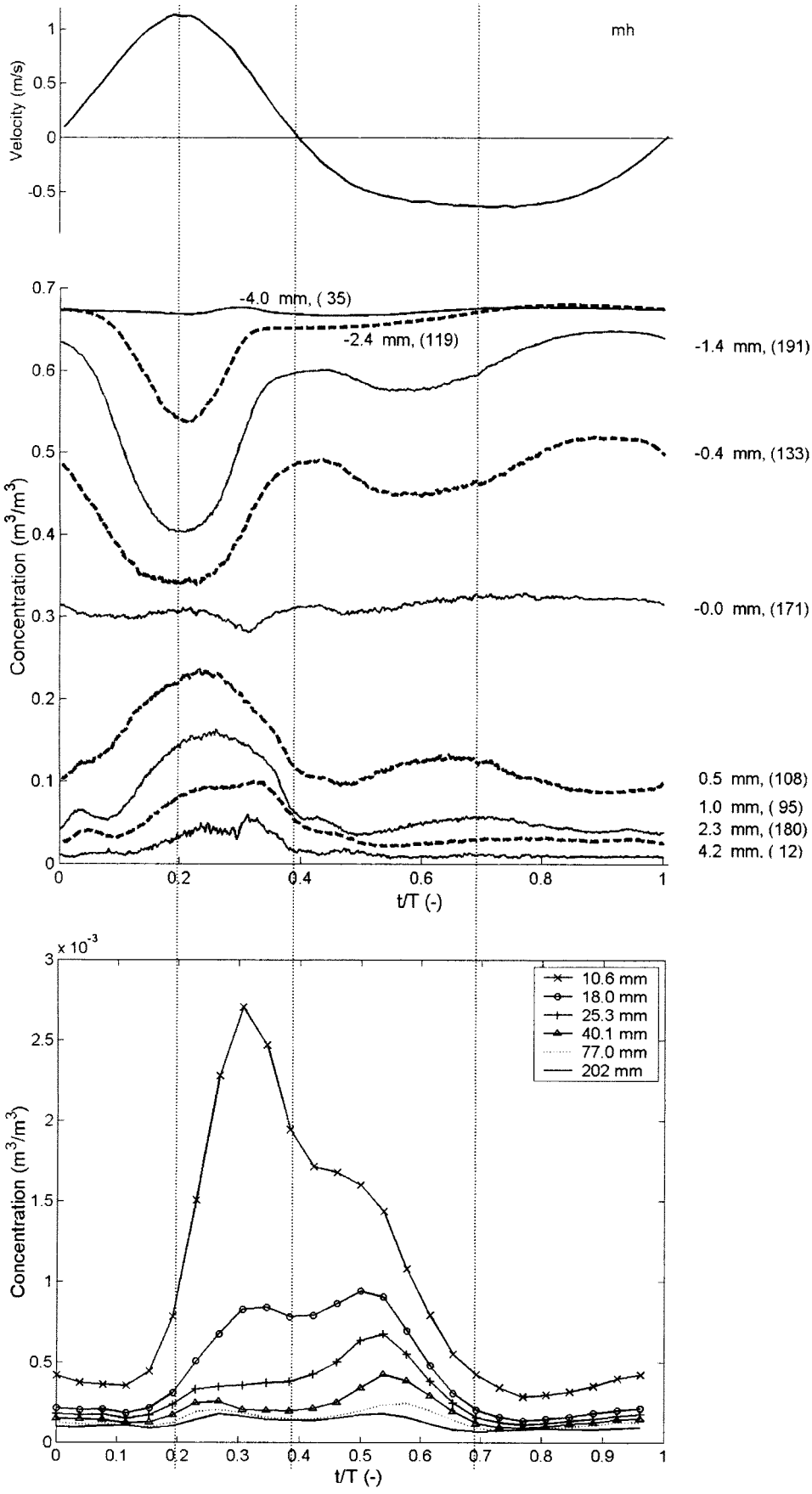

Figure 9. Measured ensemble-averaged concentrations at different elevations in the sheet flow layer for condition mh.

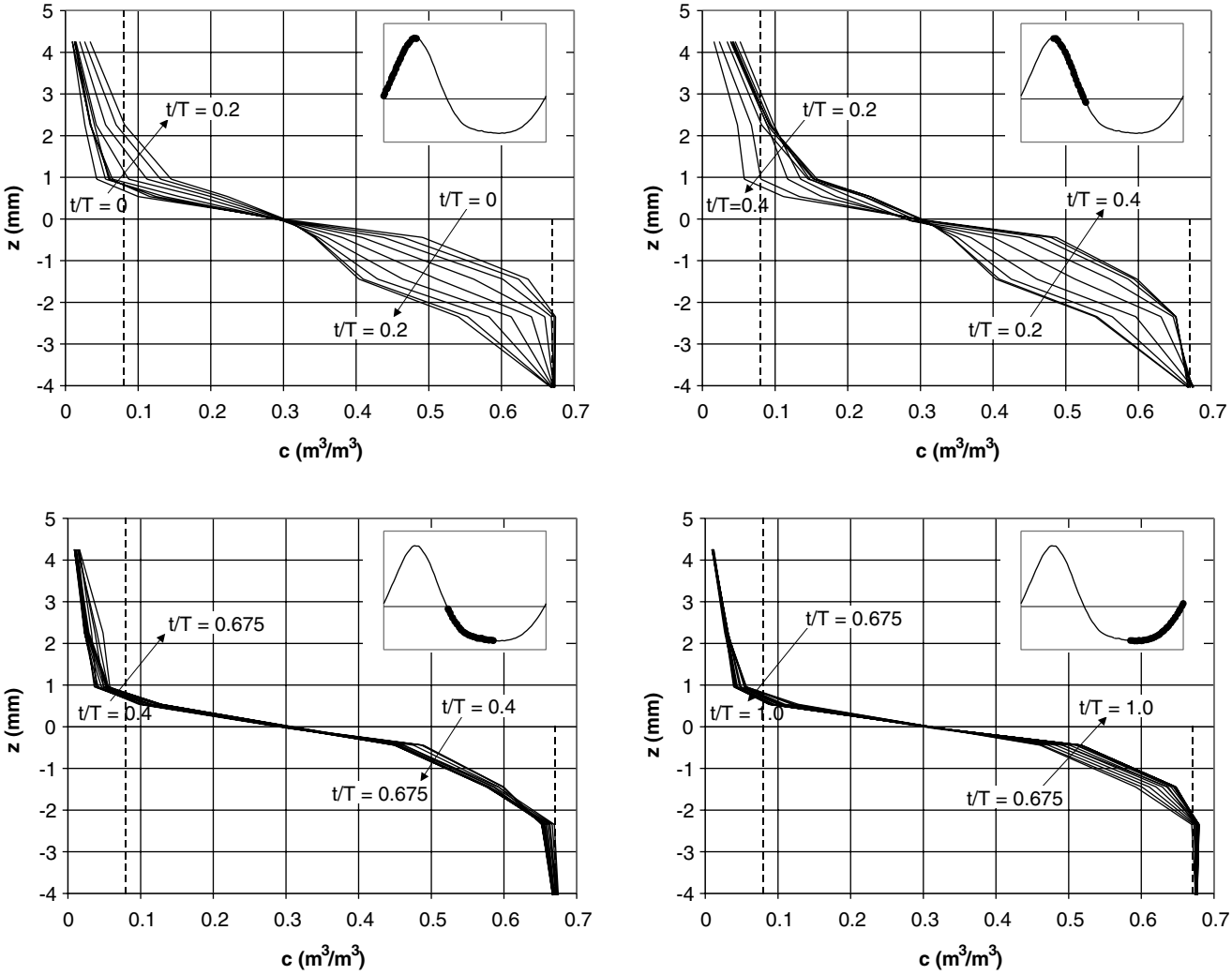

Figure 10. Vertical sediment concentration profiles inside the sheet flow layer at different phases during the wave cycle for condition mh.

might be an artifact of the sampling volume of the CCM (which has a thickness of 1–1.5 mm).

[42] It is difficult to compare the measured time-dependent concentrations directly with the time-dependent concentrations measured by *Ribberink and Al-Salem* [1995] in a large OWT, because test conditions were similar but not exactly the same. However, the time-dependent pattern of the concentrations in the sheet flow layer under waves, as presented in Figure 9, is very similar to that observed by *Ribberink and Al-Salem* [1995] and to those observed in other OWT experiments under different conditions [e.g., *Dohmen-Janssen et al.*, 2002]. Therefore a more integrated parameter, i.e., the sheet flow layer thickness, will be used to make a direct comparison between the results under waves and in uniform oscillatory flows (see section 5.2).

[43] The lower panel of Figure 9 shows the ensemble-averaged concentrations at 5 elevations in the suspension layer. These measurements were obtained with an ABS, which acquires nearly instantaneous vertical profiles, so measured phase differences are accurate and do not rely upon assumptions typically required when interpreting pump-sampling systems. This figure shows that at 10.6 mm above the bed the peak in concentration occurs after the moment of maximum velocity and later than in the sheet flow layer. This is caused by the time required to entrain sediment into the flow. At higher elevations the maximum concentration occurs after flow reversal, i.e., under the trough of the wave. This means that the sand that causes this concentration peak will be transported in the direction opposite to the wave propagation, which shows that the phase of the concentration is an important parameter for the sediment flux. The patterns of suspension close to the seabed are qualitatively consistent to the "onshore" suspension events observed in the field by *Dick et al.* [1994], and the patterns further from the bed are similar to their "offshore" suspension events.

5.2. Time-Dependent Concentration Profiles and Sheet Flow Layer Thickness

[44] Time-dependent concentrations in the sheet flow layer are presented in a different way in Figure 10, which shows vertical concentration profiles at different phases during the wave cycle. For example, the upper left-hand

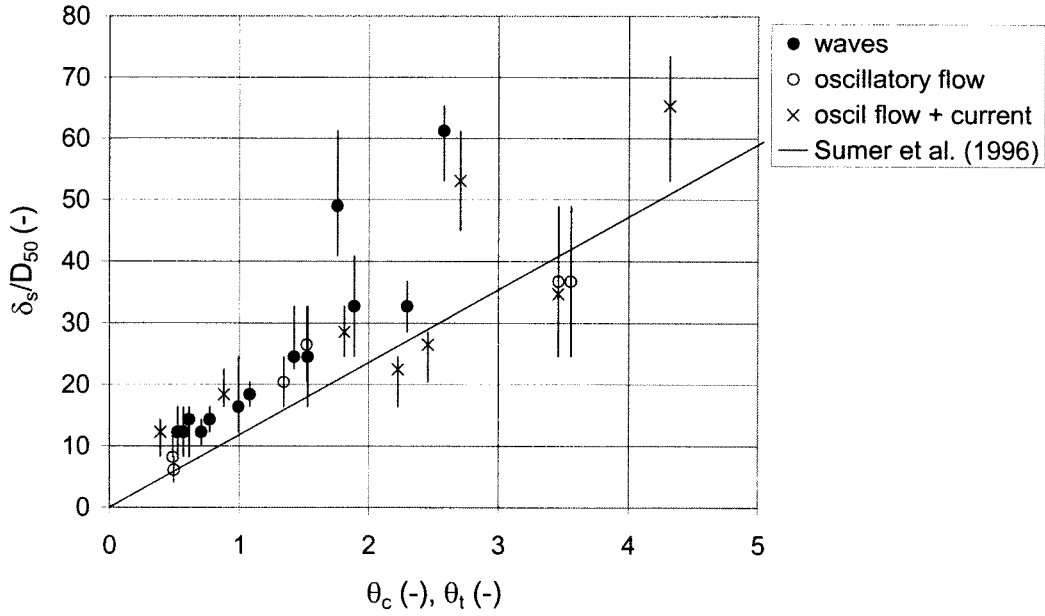

Figure 11. Sheet flow layer thickness under the crest and the trough of the wave (i.e., at maximum positive and negative velocity) as a function of Shields parameter: comparison between measurements under waves and in horizontal uniform oscillatory flow and an empirical expression for steady flow derived by *Sumer et al.* [1996].

panel shows that from t/T = 0 to t/T = 0.2 (acceleration phase under the crest of the wave) more and more sediment is being picked from below z = 0 and entrained into the flow (above z = 0) and the thickness of the sheet flow layer increases. When the flow decelerates (t/T = 0.2–0.4; upper right-hand panel) the sand settles out and the sheet flow layer thickness decreases again. These results indicate that the concentration in the sheet flow layer is directly and nearly simultaneously related to the near-bed velocity.

[45] Generally, the sheet flow layer is defined as the layer where intergranular forces are important [e.g., *Bagnold*, 1956]. Therefore in this study the top of the sheet flow layer is defined at the level where the concentration is equal to 0.08 m^3/m^3, which corresponds to a concentration for which the distance between uniform spheres in rhombohedral packing is equal to the sphere diameter. It can be expected that for higher concentrations intergranular forces become important.

[46] At t/T = 0.2 (maximum crest velocity) the concentration at z = −4 mm is equal to the still bed value, while the concentration at z = −2.4 mm is smaller than the still bed value. This means that at this instant the bottom of the sheet flow layer is located between z = −2.4 mm and z = −4 mm. The concentration profile reaches a value of 0.08 m^3/m^3 at about z = +2.5 mm, which is the top of the sheet flow layer. This means that at this instant the sheet flow layer has a thickness of about 5–7 mm.

[47] Under the trough of the wave (lower panels) the velocities remain lower than under the crest of the wave. Consequently, the sheet flow layer is thinner and shows a smaller variation during this part of the wave cycle. For example at maximum trough velocity (t/T = 0.675) the bottom of the sheet flow layer is located between z = −1.4 mm and z = −2.4 mm and the top of the sheet flow layer is located at about z = +1 mm. Thus at this instant the sheet flow layer has a thickness of about 2.5–3 mm.

[48] Note that the thickness of the sheet flow layer does not decrease down to zero when the velocity decreases to zero. This may partly be caused by the fact that sand does not react *fully* instantaneously to changes in near-bed velocity. However, it will also be influenced by the fact that the measured concentration is the average value over the sampling volume of the CCM, which has a height of about 1–1.5 mm. Even for a still bed, the measured concentration will show a continuous distribution decreasing from the still bed value (0.67) when the sampling volume is completely buried under the sand to zero concentration, when the sampling volume is completely above the sand bed. Indeed, it was found that for conditions with no sheet flow layer, CCM measurements showed a decrease in concentration from 0.67 to 0.08 over about 1–1.5 mm. Thus, values of sheet flow layer thickness less than 1.5 mm are not considered to be very accurate.

[49] Based on these considerations the thickness of the sheet flow layer has been determined from the concentration profiles under the maximum crest and maximum trough velocity for all three conditions for which detailed CCM measurements were carried out (i.e., me, mf, and mi). In addition, the sheet flow layer thickness has been determined for 4 conditions, for which just one half-hour run was carried out (mk, ml, mm, and mn). During these tests the CCMs have been moved up and down through the sheet flow layer to determine the thickness of the sheet flow layer.

[50] Values of the sheet flow layer thickness under the maximum crest and maximum trough velocity derived in this way are normalized by the mean grain size and plotted in Figure 11 against the maximum value of the Shields parameter θ under the crest or the trough of the wave,

respectively. This figure also shows values of sheet flow layer thickness, measured in an OWT with and without a net current superimposed and an expression for the nondimensional sheet flow layer thickness as a function of θ, derived by *Sumer et al.* [1996], based on observations in steady flow. For the measurements, the (calculated) maximum values of θ under the crest and under the trough of the wave (i.e., θ_c and θ_t) were presented in Table 1.

[51] The figure shows that the sheet flow layer is several grain diameters thick (10–60) and that values of the sheet flow layer thickness under waves are very similar to those in OWT flows and to those in steady flow. A linear relation between the nondimensional sheet flow layer thickness and the Shields parameter seems to be a reasonable approximation.

6. Grain Velocities Inside the Sheet Flow Layer

[52] Grain velocities in the sheet flow layer were determined from a cross-correlation between the two concentration signals: the time lag for which a peak in cross-correlation is observed (Δt) determines the horizontal grain velocity u_g, because the distance between the probes is fixed (Δx = 15 mm): $u_g = \Delta x/\Delta t$. Velocities were calculated at different elevations above the base of the sheet flow layer, as determined by the average elevation of each concentration bin. First, the concentrations signals were high-pass filtered. In order to determine the velocity within the wave cycle, each wave period was divided into 36 intervals. For each phase interval of each wave within a bin, the cross-correlation of the two concentration signals was determined. Next the cross-correlations of all the waves in a bin were averaged per phase interval, in order to determine the ensemble-averaged cross correlation. For more details about this correlation technique, see the work of *McLean et al.* [2001].

[53] *Ensemble-Averaged Time Series:* Figure 12 shows the ensemble-averaged grain velocities at different elevations inside the sheet flow layer, together with the free-stream velocity (measured by ADV at about 0.1 m above the bed) for condition mh. Grain velocities could only be determined under the crest of the wave: no clear peak in cross-correlation was observed under the trough of the wave. It is expected that this is caused by the fact that both the sheet flow layer under the trough is much thinner and the velocities are much lower.

[54] The figure shows that the grain velocities inside the sheet flow layer are relatively high: even in the pick-up layer (z < 0 mm) the grain velocity is still about 50% of the free-stream velocity. Because the concentrations in the pick-up layer are very high, this leads to high sediment fluxes in this region, as will be shown later.

[55] The velocity at z = +1.0 mm and +2.3 mm clearly leads the free-stream velocity. However, in the pick-up layer the peak in grain velocity seems to occur later than just above the bed. This might be caused by the fact that at this low level the sand only starts moving when enough sediment has been picked up from the bed.

[56] These results are similar to observations by *McLean et al.* [2001] in a large OWT. However, a direct comparison between the results is not possible, since McLean et al. applied sinusoidal oscillatory flow in combination with a net current rather than asymmetric oscillatory flow. Notice that McLean et al. were able to measure grain velocities under the trough of the wave as well as under the crest, probably due to the fact that their oscillatory motions were less asymmetric, resulting in a higher trough velocity, concentration, and sheet flow layer thickness than in the present experiments.

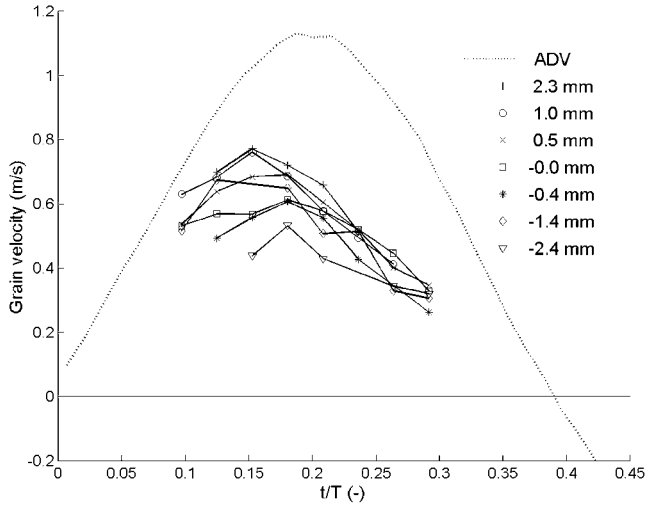

Figure 12. Grain velocities under the crest of the wave inside the sheet flow layer for condition mh.

7. Comparison of Measured Velocity, Concentration, and Sediment Flux Profiles With Theories

[57] Measured velocities, concentrations and resulting sediment fluxes are next compared with predictions of two distinct, existing models. The first is the time-dependent 1DV sediment transport model developed by *Ribberink and Al-Salem* [1995, hereafter RA95] that describes the distribution of flow velocity and suspended sediment concentration in an oscillating boundary layer. The second is the collisional grain flow model of *Jenkins and Hanes* [1998, hereafter JH98]. JH98 describes the distribution of grain and fluid velocities and sediment concentrations over a steady, unidirectional, sheet flow layer. Neither of these models is expected to fully describe our sheet flow observations, but they provide two extremes in their assumptions regarding the physical processes in sheet flow. RA95 models the boundary layer as a pure turbulent fluid, with an effectively increased roughness due to the sheet flow. JH98 is a two-phase model in which the granular interactions are described by application of kinetic theory. Before presenting the results, the models will be briefly summarized below.

7.1. 1DV Time-Dependent Suspension Model

[58] RA95 calculates the velocity in the boundary layer of a uniform horizontal oscillatory flow ($\partial u/\partial x = 0$; w = 0). Thus rather than the boundary layer flow under progressive waves, the model describes the boundary layer as present in an OWT. It solves the 1DV Navier–Stokes equation, using the free-stream velocity as a boundary condition. At the

lower boundary, the velocity is assumed to be equal to zero at $z_0 = k_s/30$, with k_s the roughness height. The Prandtl mixing length is applied to calculate the (time-dependent) turbulent eddy viscosity ν_t:

$$\nu_t(z,t) = l_m^2 \left| \frac{\partial u(z,t)}{\partial z} \right| = (\kappa z)^2 \left| \frac{\partial u(z,t)}{\partial z} \right| \quad (4)$$

Here l_m is the mixing length, which is equal to κz with κ the Von Karman constant ($\kappa = 0.4$).

[59] Suspended sediment concentrations are calculated from a mass balance, using an advection-diffusion approach. Boundary conditions for the sediment concentrations are: zero vertical sediment flux at the upper boundary and an imposed reference concentration at the lower boundary (reference level = 2 D_{50}), according to the expression of *Engelund and Fredsøe* [1976].

[60] The model is based on the assumption that concentrations are so low, that the flow velocity is not influenced by the presence of the sediment and that the vertical sediment velocity is equal to the settling velocity of a single sediment particle. Specific sheet flow processes, like sediment–flow interaction and grain–grain interaction, are not included.

7.2. Sheet Flow Model

[61] JH98 applies the kinetic theory of grain flows to formulate a theory for a two-phase, unidirectional sheet flow. The theory was developed to describe intense bed load sediment transport under conditions during which the collisions between grains dominate the momentum transport. Momentum and energy conservation equations are formulated for each phase. JH98 specifies a standard eddy viscosity profile to describe the turbulent shearing of the fluid. The kinetic theory of granular flow is used to formulate the stresses in the granular phase that result from intergranular collisions. The fluid and granular phases are coupled through the drag that results from the velocity difference of the mean motion of the fluid and that of the particles. The lower boundary that separates moving from immobile grains is treated as a phase transition, which results in a boundary condition that specifies $c_b = 0.55$, which is the maximum concentration at which a randomly packed assembly of spheres can shear without dilation. The momentum and fluctuational energy conservation equations are solved numerically along with specific boundary conditions to provide the profiles of concentration, velocity, and fluctuational energy. As JH98 was developed to describe steady, unidirectional flows, it might be expected to apply to oscillatory flows during instances of maximum (and minimum) velocity when the fluid acceleration is relatively small.

7.3. Model Data Integration

[62] Unfortunately, the CCM measurement technique only allowed grain velocities to be measured under the crest of the waves. Therefore, a comparison is made between measurements and predictions of the two models at the phase of the maximum free-stream velocity for condition mh (i.e., t/T = 0.2).

[63] In RA95 the level z = 0 corresponds to the undisturbed bed. Therefore, all levels in the calculations of the suspension model are shifted down 4.0 mm, such that the undisturbed bed is at z = −4.0 mm, which corresponds to the undisturbed bed in the measurements at the phase of the maximum free-stream velocity (see Figure 10). The suspension model only calculates concentrations from the reference level z_a above the undisturbed bed, upward ($z_a = 2\ D_{50} = 0.49$ mm). Therefore, results of the suspension model are only shown for $z \geq -3.5$ mm. At the upper boundary a velocity is imposed in the form of a second-order Stokes velocity:

$$u(t) = u_1 \sin(\omega t) + u_2 \left(2\omega t - \frac{1}{2}\pi \right) \quad (5)$$

[64] The velocity measured by ADV at 0.1 m above the bed is analyzed to determine u_1 and u_2. For run mh the following values are found: $u_1 = 0.90$ m/s and $u_2 = 0.19$ m/s. Next, calculated velocities are shifted in phase such that t/T = 0 corresponds to an upward zero-crossing velocity, just as in the measurements. At the lower boundary the roughness height has to be specified. Results are shown for two different roughness heights. First a roughness height of 2.5 D_{50} is applied. This is a more or less standard value for the roughness height of a flat sand bed. However, it is often assumed that in sheet flow conditions the roughness height is much larger than 2.5 D_{50}. Based on measurements of velocity and concentration profiles in sheet flow conditions in an OWT, *Dohmen-Janssen et al.* [2001] found that in oscillatory sheet flow the roughness height is of the order of the sheet flow layer thickness. This is in agreement with observations by *Sumer et al.* [1996] and *Wilson* [1989], for example, for steady flow. Therefore, model calculations are also carried out with an imposed roughness height that is equal to the measured sheet flow layer thickness for this case (i.e., $k_s = 6$ mm).

[65] The higher roughness leads to a higher bed shear stress. Because the imposed velocity at the top is the same in both cases, an increased bed shear stress leads to decreased velocities close to the bed. In addition, the increased shear stress leads to increased sediment concentrations.

[66] JH98 is compared here with measurements under waves by assuming that the sheet flow layer behaves in a quasi-steady manner. This means that at each instant during the wave cycle the velocity and concentration in the sheet flow layer are assumed to be instantaneously related to the driving force (i.e., the shear stress or the free-stream velocity). Obviously, this is not exactly the case, since the flow in the wave boundary layer leads the free stream. However, it is a reasonable approximation at the phase of the maximum free-stream velocity, when the accelerations are small. Moreover, measurements showed that in the sheet flow layer, concentrations are directly and indeed nearly simultaneously related to the near-bed velocity (Figures 9 and 10), indicating that inside the sheet flow layer the assumption of quasi-steadiness is reasonable.

[67] The JH98 model can be driven by a shear stress (Shields parameter) or by the velocity at the top of the sheet, which in this case is defined as the level where the concentration is equal to 0.01 m^3/m^3. Unfortunately, neither of these two parameters were directly measured in the experiments. Therefore, the RA95 model with increased roughness is used to yield the velocity at the top of the

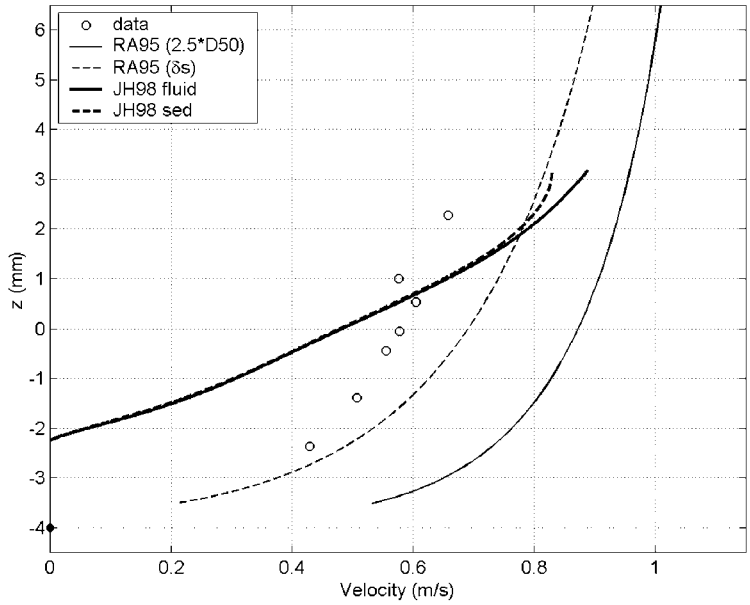

Figure 13. Predicted and measured velocity profiles in the sheet flow layer at the phase of peak velocity.

sheet. It turns out that the velocity in the suspension model does not vary a lot with height at levels higher than about 10 mm above the undisturbed bed. Therefore the value of the velocity calculated by RA95 with increased roughness at 10 mm above the undisturbed bed is imposed as the velocity at the top of the sheet in the sheet flow model. Increased roughness is used to give more realistic results in sheet flow conditions.

[68] In order to compare the measurements to the predictions of JH98, the level z = 0 (initial still bed) is determined in the same way as in the measurements, i.e., by shifting the level z = 0 until the total amount of sand missing below z = 0 is equal to the total load above z = 0.

7.4. Results

[69] Comparisons between the measurements and the model results are presented in Figures 13, 14, and 15. Figure 13 presents velocity profiles in the lower 10 mm above the undisturbed bed (no velocities were measured between z = 2.4 mm and z = 100 mm). Figures 14 and 15 present the concentration and sediment flux profiles in the lower 0.1 m above the undisturbed bed on log–log scale. In order to show the concentrations and fluxes in the pick-up layer (i.e., at negative z-values), they are plotted against z', with $z' = z + 4$ (mm). Thus the bottom of the sheet flow layer is at $z' = 0$ in these two plots.

[70] Measured sediment fluxes are determined as the product of concentrations measured by CCM and grain velocities, derived from cross-correlations between the CCM signals. Figure 15 also includes an estimate of the measured suspended sediment flux. Since no velocity measurements are available below z = 0.1 m in the suspension layer, the suspended sediment flux is estimated from time-dependent suspended sediment concentrations measured by ABS and time-dependent velocities calculated by RA95 with increased roughness.

7.4.1. Sheet Flow Layer

[71] Figure 13 shows that RA95 with a roughness of 2.5 D_{50} predicts much higher velocities than the measured grain velocities inside the sheet flow layer. Note that the model predicts fluid velocities, while the measurements represent the velocity of the grains. However, the JH98 model indicates that the difference between the two phases is minor. Imposing an increased roughness leads to reduced velocities in the near-bed region and improved agreement with the measurements. This indicates that velocities inside the sheet flow layer are reduced, compared to velocities above a flat sand bed without a sheet flow layer. This is in agreement with earlier observations from an OWT, indicating that near-bed processes in purely oscillatory flow are indeed similar to those under waves.

[72] The JH98 model predicts a much thinner sheet low layer than observed in the measurements: the velocities go to zero at z = −2.2 mm and the top of the sheet flow layer (the level where the concentration is equal to 0.01 m^3/m^3) is located at z = +3.2 mm, yielding a sheet flow layer thickness of 5.4 mm. Using this definition for the top of the sheet flow layer would result in a sheet flow layer in the measurements of about 9–11 mm. Consequently, the sheet flow model predicts a much larger shear than observed in the measurements. The fact that the velocities go to zero closer to the initial bed than in the measurements may partly be caused by the fact that in this model it is assumed that particles cannot shear at concentrations higher than 0.55 m^3/m^3, while in the measurements grains are still moving relatively fast when the concentration is equal to 0.53 m^3/m^3.

[73] Figure 14 shows that the near-bed concentrations predicted by RA95 are much lower than the measured

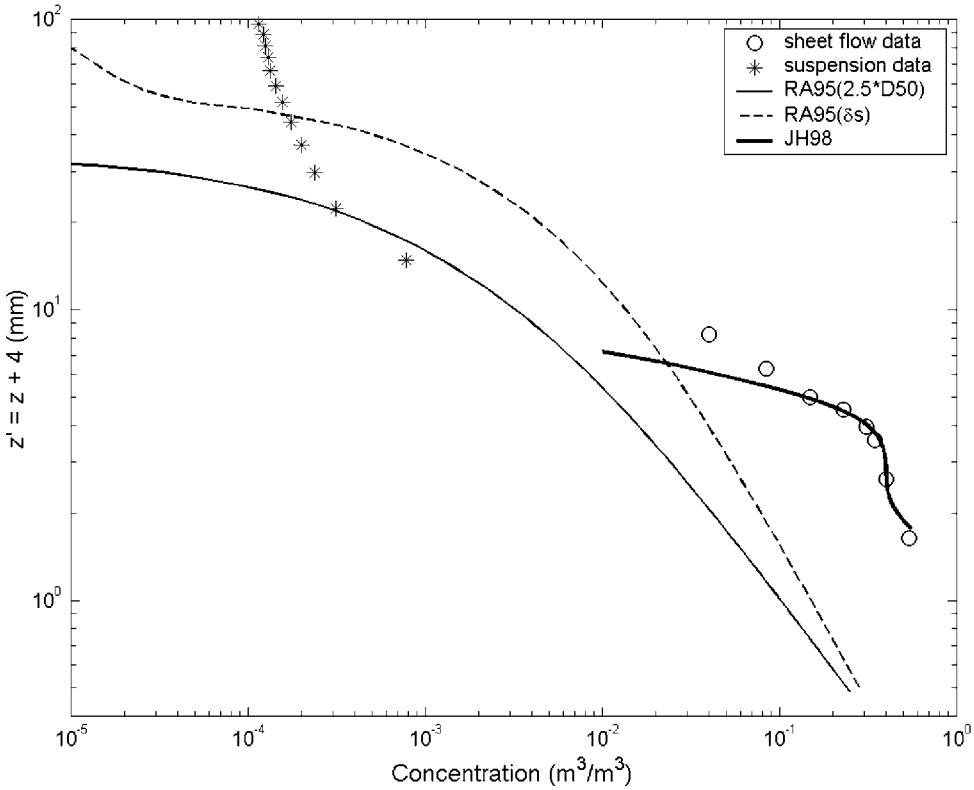

Figure 14. Predicted and measured concentration profiles at the phase of peak velocity.

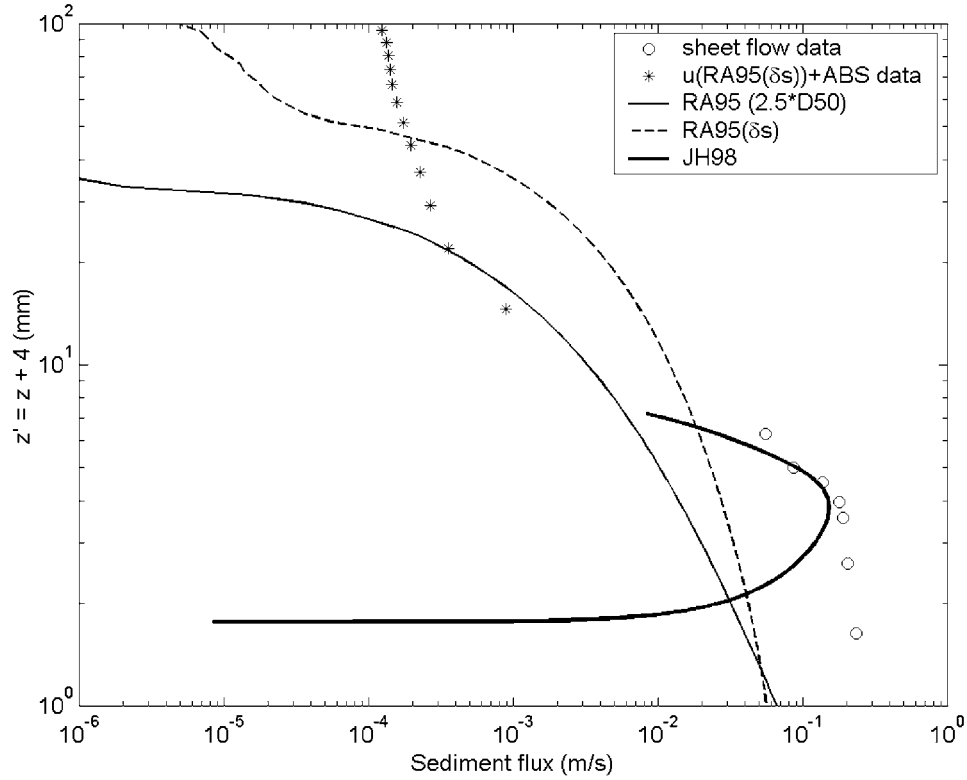

Figure 15. Predicted and measured sediment flux profiles at the phase of peak velocity.

concentrations. This is not surprising, since this model does not include any sheet flow processes, but just calculates a reference concentration at 2 D_{50} above the undisturbed bed and the concentration profile above it based on an advection-diffusion approach. An increased roughness leads to increased concentrations due to the larger shear stress and thus higher mixing coefficient.

[74] The JH98 model shows surprisingly good agreement with the measured concentrations. This model does not predict concentrations higher than 0.55 m^3/m^3, since this value is used as boundary condition, where the velocities go to zero. Higher in the sheet flow layer ($z > +1$ mm; $z' > 5$ mm), the model predicts smaller concentration than observed in the measurements. This is probably caused by the fact that this model does not include any mixing of sediment due to turbulence, which starts to become important in this region, where the concentrations are relatively small.

[75] Figure 15 shows that the measured sediment flux inside the sheet flow layer continues to increase toward the bed. However, near $z = -4.0$ mm ($z' = 0$) the sediment flux must be zero, because this is the level of the undisturbed bed. Due to the largely underestimated concentrations, the sediment fluxes in the sheet flow layer predicted by RA95 are much smaller than the measurements. JH98 predicts sheet flow fluxes that are very similar in magnitude to the measured fluxes. However, they decrease to zero faster than in the measurements (over a thinner sheet flow layer).

7.4.2. Suspension Layer

[76] As shown before (Figures 6 and 9), Figure 14 shows that the suspended sediment concentration is much smaller than the concentration in the sheet flow layer. Figure 15 shows that, as a consequence, the suspended sediment flux is more than an order of magnitude smaller than the sediment flux in the sheet flow layer. This means that—at least under the crest of the wave—a large part of the sediment transport is concentrated very close to the bed, inside the sheet flow layer. This was observed before in uniform oscillatory flow [e.g., *Dohmen-Janssen et al.*, 2002]. However, it is important to notice that this also seems to be the case under waves, even though the suspended sediment concentrations under waves are larger than in uniform oscillatory flow (see Figure 8).

[77] The suspended concentration and sediment flux profiles predicted by RA95 are very different from the measured profiles. The predicted concentrations and sediment fluxes decrease much faster with height than in the measurements, suggesting that either additional mixing is present in the experiments that is not included in the model, or that there are sediment grading effects in the experiments that are not included in the model.

8. Net Sediment Flux and Comparison With Measured Total Net Transport Rate

[78] Vertical integration of the sediment flux profile, presented in Figure 15, yields the sediment transport rate under the crest of the wave in the lower 100 mm above the bed. The transport rate above that level has been estimated from extrapolation, by fitting a linear profile through the upper part of the flux profile ($z > 60$ mm). The transport rate between the lowest level in the suspension layer ($z = 10.8$ mm) and the highest level in the sheet flow layer ($z = 2.3$ mm) has been estimated by assuming a power law distribution of the flux between these levels. As before, the top of the sheet flow layer is defined as the level where the concentration is equal to 0.08 m^3/m^3, which is at approximately $z = 2.3$ mm in this case. This gives the following estimates of the transport rate under the crest of the wave in the different layers:

$$\begin{aligned}
&\text{suspension layer } (z > 2.3\,\text{mm}): && q_{sc,sus} = 94{*}10^{-6}\,m^2s (= 9.5\%)\\
&\text{sheet flow layer } (z < 2.3\,\text{mm}): && \underline{q_{sc,sf} = 896{*}10^{-6}\,m^2s (= 90.5\%) +}\\
&\text{total}: && q_{sc} = 991{*}10^{-6}\,m^2s (= 100\%)
\end{aligned}$$

[79] Apparently, under the crest of the wave, the suspended sediment transport rate is less than 10% of the total. Moreover, it was found that approximately 95% of the total transport rate is located in the lower 15 mm above the undisturbed bed ($z = -4$ mm to $z = +11$ mm). However, the large vertical gradients in this region in combination with the relatively large inaccuracy in the elevation of the CCM (±1 mm) and the uncertainties in the values of the concentration and the grain velocities lead to large uncertainties in the value of the transport rate. It is estimated that due to these uncertainties the transport rate derived from integration of the flux profile may vary with about a factor 0.5–1.6.

[80] Because grain velocities and thus sediment fluxes could not be determined under the trough of the wave, the *net* sediment flux or *net* sediment transport rate cannot be determined directly from the flux measurements. However, both in the past and for the present flume tests it was found that a linear relation between the transport rate and the third power of the instantaneous near-bed velocity is a reasonable assumption for the sheet flow layer. Therefore, the sediment flux measurement under the crest of the wave and the measured time-dependent near-bed velocity are used to calculate the time-dependent transport rate over the full wave cycle. Averaging over the wave yields the following estimate of the net transport rate: $\langle q_{s,\,flux} \rangle = 70.7 \times 10^{-6}$ m^2/s (±50–60%). This value can be compared with the net transport rate, derived from the mass conservation technique $\langle q_{s,mc} \rangle$ (section 3.2), which for the present condition (mh) was equal to 42.9×10^{-6} m^2/s (±40%).

[81] There are several possible sources of error that may contribute to this discrepancy. For example, the relation between q_s and u^3 and/or the fact that a slightly different time-dependent velocity may lead to relatively large differences in the mean value of $\langle u^3 \rangle$, especially for the relatively symmetric flow velocity of condition mh. Moreover, the value of the bed concentration c_b, measured by CCM, was found to be 0.67 (corresponding to a porosity of the sand bed of 0.33). This is considered to be rather high, resulting in high estimates of the sediment flux. This might be caused by an incorrect estimate of the CCM calibration factor. A value of c_b of about 0.6 is probably more realistic (corresponding to a porosity of 0.4). Since it is reasonable to assume that the calibration factor is constant, the concentrations in the sheet flow layer are multiplied with a factor 0.9 (0.6/0.67) to provide a better estimate of the net transport rate from the sediment flux profile.

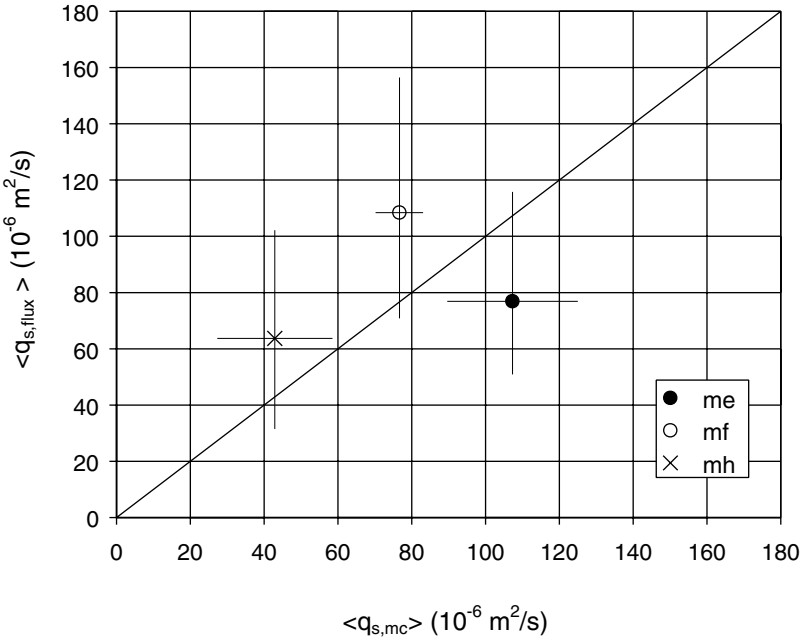

Figure 16. Comparison of net transport rates estimated from sediment flux profiles close to the bed with net transport rates derived from the mass conservation technique.

[82] The same analysis is performed for the other two conditions for which CCM measurements are carried out (i.e., me and mf). Figure 16 presents a comparison between the net transport rates derived from the mass conservation technique $\langle q_{s,mc} \rangle$ and the net transport rates derived from the sediment flux profiles $\langle q_{s,flux} \rangle$ (using $c_b = 0.6$). It is considered to be promising that the new cross-correlation technique to measure grain velocities inside the sheet flow layer yields estimates of net transport rates that are similar to the total net transport rates derived from the mass conservation technique, as indicated by the fact that the error bars cross the line of perfect agreement, despite the assumptions and inaccuracies to calculate the sediment flux in the sheet flow layer.

9. Conclusions

[83] Near-bed sediment transport measurements have been presented from experiments that were carried out under prototype wave conditions in a large wave flume. Observations of sheet flow and suspension processes and transport rates under propagating surface waves were compared with earlier observations of similar phenomena in OWTs, and with different theories. This lead to the following conclusions:

[84] For the first time it has been possible to measure detailed sediment concentrations and grain velocities (from a cross-correlation of two concentration signals) at different elevations inside the sheet flow layer under prototype waves. This is an important and promising result for possible future research in the field. Still, grain velocities could only be determined under the crest of the wave. It is expected that due to the asymmetry in velocity both the thickness of the sheet flow layer and the grain velocities under the trough of the wave were too small to yield significant cross-correlations.

[85] The behavior of the sheet flow layer under waves is qualitatively similar to that in horizontal OWT flows:

1. Large concentration gradients exist over the (thin) sheet flow layer. The gradients within the sheet flow layer are at least one order of magnitude greater than suspended sediment concentration gradients that typically occur further away from the bed.

2. The sheet flow layer under waves has a thickness of order(10) grain diameters, ranging from approximately 10 to 60. These values are very similar to those in OWTs and are well represented by the empirical relation of *Sumer et al.* [1996] for steady flow.

3. Below the initial bed level, a pick-up layer is observed. In this layer the concentration is equal to the bed concentration when the velocity is small. When the velocity increases, the concentrations decrease, because the sediment dilates due to dynamic interactions.

4. Above the initial bed level is the upper sheet flow layer where concentrations increase as the velocity increases, because sediment is entrained from below into the flow. When the velocity decreases again, concentrations decrease too.

5. The asymmetry in near-bed velocity (larger crest velocities than trough velocities) is reflected in the concentrations (both in the pick-up layer and in the upper sheet flow layer).

6. Concentrations inside the sheet flow layer are nearly instantaneously related to the near-bed velocity. This is caused by the fact that the sheet flow layer is relatively thin and located close to the bed, resulting in a quick sediment response.

[86] Time-dependent suspended sediment concentrations above the sheet flow layer are an order of magnitude smaller than the concentrations within the sheet flow layer. They show increasing phase lags with increasing distance above the bed, with the maximum suspended concentration occur-

ring under the trough of the wave for levels higher than about 18 mm above the bed.

[87] Time-averaged suspended sediment concentrations under waves are much higher than in OWT flows under similar conditions. This might be caused by suppression of a vertical velocity component in an OWT due to the rigid upper lid. However, even under waves, the contribution of the suspended load to the total transport rate in sheet flow conditions is still of minor importance.

[88] Grain velocities inside the sheet flow layer are relatively high: even inside the pick-up layer, grain velocities are about half the value of the free-stream velocity (i.e., outside the wave boundary layer).

[89] Due to the large grain velocities and large sediment concentrations, sediment fluxes in the sheet flow layer are much larger than suspended sediment fluxes. Estimates of net transport rates in the sheet flow layer, derived from measured sediment fluxes under the crest of the wave indicate that the transport rate inside the sheet flow layer is similar to the total net transport rate. This indicates that most of the sediment transport is taking place inside the sheet flow layer, i.e., very close to the bed. This is in agreement with observations in horizontal oscillatory flows. Apparently, also under waves the contribution of the suspended load to the total transport rate in sheet flow conditions is still of minor importance, despite the relatively larger suspended sediment concentrations.

[90] Total net transport rates determined from successive bed profiles showed a linear relation with the third power of the fluid velocity above the boundary layer. This third-power dependency is consistent with previous observations in OWT flows. However, magnitudes of net transport rates under waves are approximately 2.5 times larger than found in previous OWT experiments. This is expected to be (partly) caused by the onshore-directed boundary layer streaming, which is present under waves and absent in OWTs. Despite the small value of this streaming, compared to the maximum velocity, it might have a large effect on the net transport rate, especially since it is located inside the boundary layer, which means that it occurs in the sheet flow layer, where sediment concentrations are very high.

[91] Various features of the observations are described by two very different models: a time-dependent suspension model with enhanced boundary roughness (RA95), and a steady two-phase collisional grain flow model (JH98). RA95 is successful in describing the velocity profile using an enhanced roughness approximately equal to the measured sheet flow thickness. JH98 appears to describe the main features of the sheet flow layer such as the profiles of concentration and velocity. Considering that we have not modified the theory to reflect the oscillatory nature of the flow, we find this agreement to be quite encouraging. However, there were some discrepancies between the observations and the JH98 model, particularly near the upper and lower surfaces of the sheet flow. Near the upper surface, the collision-based theory does not describe the effects of fluid turbulence upon the suspension of sediment. Near the lower boundary, the assumed concentration of 0.55, which originated from a consideration of homogeneous spheres, is clearly lower than the measured concentrations of natural sand grains.

[92] The present measurements in combination with previous measurements and theories provide compelling evidence that sheet flow is a highly important process in nature under certain conditions. However, we recognize that investigations into the detailed dynamics of sheet flows are still just beginning; theories and models must be considered preliminary until more detailed measurements can be obtained for verification. Several features of oscillatory sheet flows are still not adequately described. Some of these include: the fluid velocity inside the sheet flow layer; the velocity field of the grains over the entire cycle; the nature of the boundary separating moving and immobile grains; the transition between collisional grain interactions and fluid–grain suspension interactions; the effects of natural, graded sediment upon collisions, packing, the actual shear stress and effective drag coefficient; the presence and importance of combined wave–current effects and boundary layer drift velocities; the conditions under which sheet flows occur in natural coastal environments; the effects of wave groups and random waves; effects of pore pressure; and the effects of fine sediments or biological matter within the bed.

Notation

c	sediment concentration, m^3/m^3
c_a	reference concentration at z_a, m^3/m^3
c_b	concentration of the sand bed, m^3/m^3
c_m	time-averaged concentration, m^3/m^3
D_{50}	median grain size, m
H	wave height, m
k_s	bed roughness height, m
q_s	sediment transport rate, m^2/s
$\langle q_s \rangle$	net sediment transport rate, m^2/s
t	time, s
T	wave period, s
u	horizontal velocity, m/s
u_*	friction velocity, m/s
u_c	horizontal orbital velocity under the crest of the wave, m/s
u_m	time-averaged horizontal velocity, m/s
u_g	horizontal grain velocity, m/s
u_{rms}	root mean square value of horizontal orbital velocity, m/s
u_t	horizontal orbital velocity under the trough of the wave, m/s
w	vertical velocity, m/s
w_s	settling velocity of a single sediment particle, m/s
x	distance from wave paddle (in wave propagation direction, i.e., along the flume), m
z	level above the bed, m
z_0	$k_s/30$, m
z_a	reference level for the concentration, m
α	concentration decay parameter $\alpha = w_s/\kappa u_*$, –.
δ_s	sheet flow layer thickness, m.
ε_0	porosity, –.
ε_{sz}	vertical sediment diffusivity, m^2/s.
ϕ	sediment flux, m/s.
κ	Von Karman constant (=0.4).
θ	Shields parameter, –.
ρ	density of water, kg/m^3.
ρ_s	density of the sediment, kg/m^3.
ω	angular frequency of the wave (=$2\pi/T$), rad/s.

[93] **Acknowledgments.** The experiments were made possible by the University of Hannover and the ForschungsZentrum Kste through the Human Capital and Mobility Program of the EU. The analysis was carried out with financial support of the Coastal Sciences Program of the U.S. Office of Naval Research, the U.S. National Science Foundation, the Dutch Ministry of Transport, Public Works and Water Management (National Institute for Coastal and Marine Management/RIKZ) through the research program COAST*2000 (contract no. 22990559), and the EU project SEDMOC (MAST-III, project no. MAS3-CT97-0115). We appreciate the assistance of the staff of the GWK as well as the tireless help from students Vadim Alymov, Yeon-Sihk Chang, Beth Cranston, Tim Maddux, Charlotte Obhrai, Marieke Vuurboom, and Theo Westgeest. Steve McLean helped plan, design, and carry out the experiments and also developed the CCM velocity measurement technique. Jan Ribberink set the stage for this research through his group's prior research on sheet flows, and he was instrumental in obtaining the funding for these experiments. Chris Vincent also helped obtain funding and provided useful guidance during the experiment and the analysis of results. All of the people mentioned above as well as Peter Nielsen and Alexander Khabidov contributed to preliminary discussions of these results.

References

Asano, T., Observations of granular-fluid mixture under an oscillatory sheet flow, in *Proc. 23rd Int. Conf. on Coast. Eng., New York*, pp. 1896–1909, Am. Soc. of Civ. Eng., Reston, Va., 1992.

Bagnold, R. A., The flow of cohesionless grains in fluids, *Proc. R. Soc. London, Ser. A*, *249*, 235–297, 1956.

Bosboom, J., and G. Klopman, Intra-wave sediment transport modeling, in *Proc. of the 27th Int. Conf. on Coast. Eng. 2000, Sydney*, pp. 2453–2466, Am. Soc. of Civ. Eng., Reston, Va., 2000.

Bosman, J. J., E. T. J. M. van der Velden, and C. H. Hulsbergen, Sediment concentration measurement by transverse suction, *Coast. Eng.*, *11*, 353–370, 1987.

Dibajnia, M., and A. Watanabe, Sheet flow under nonlinear waves and currents, in *Proc. of the 23rd Int. Conf. on Coast. Eng., Venice*, pp. 2015–2028, Am. Soc. of Civ. Eng., Reston, Va., 1992.

Dick, J. E., M. R. Erdman, and D. M. Hanes, Suspended sand concentration events due to shoaled waves over a flat bed, *Mar. Geol.*, *119*, 67–73, 1994.

Dohmen-Janssen, C. M., W. N. Hassan, and J. S. Ribberink, Mobile-bed effects in oscillatory sheet flow, *J. Geophys. Res.*, *106*, 27,103–27,115, 2001.

Dohmen-Janssen, C. M., W. N. Hassan, and J. S. Ribberink, Phase-lags in oscillatory sheet flow, *Coast. Eng.*, *46*, 61–87, 2002.

Engelund, F., and J. Fredsøe, A sediment transport model for straight alluvial channels, *Nord. Hydrol.*, *7*, 293–306, 1976.

Hanes, D. M., Suspension of sand due to wave groups, *J. Geophys. Res.*, *96*, 8911–8915, 1991.

Hanes, D. M., E. D. Thosteson, Y. S. Chang, C. Connor, and C. E. Vincent, Field observations of small scale sedimentation processes, in *Proc. of the 26th Int. Conf. on Coast. Eng., Copenhagen, Denmark*, pp. 2344–2352, Am. Soc. of Civ. Eng., Reston, Va., 1998.

Hanes, D. M., V. Alymov, Y. Chang, and C. D. Jette, Wave formed sand ripples at Duck, North Carolina, *J. Geophys. Res.*, *106*, 22,575, 2001.

Hoekstra, P., K. T. Houwman, A. Kroon, P. Van Vessem, and B. G. Ruessink, The NOURTEC experiment of Terschelling: Process-oriented monitoring of a shoreface nourishment (1993–1996), in *Proc. of Coast. Dyn. '94, Barcelona, Spain*, pp. 402–416, Am. Soc. of Civ. Eng., Reston, Va., 1994.

Horikawa, H., A. Watanabe, and S. Katori, Sediment transport under sheet flow condition, in *Proc. 18th Int. Conf. on Coast. Eng., Cape Town*, pp. 1335–1352, Am. Soc. of Civ. Eng., Reston, Va., 1982.

Houwman, K., and B. G. Ruessink, Cross-shore sediment transport mechanisms in the surfzone on a time scale of months to years, in *Proc. of the 25th Int. Conf. on Coast. Eng., Orlando, Fla.*, pp. 4793–4806, Am. Soc. of Civ. Eng., Reston, Va., 1996.

Inman, D. L., S. A. Jenkins, D. M. Hicks, and H. K. Kim, Oscillatory bursting over beds of fine sand, in *Ref. Ser. 86-13*, 16 pp., Scripps Inst. of Oceanogr., Univ. of Calif., San Diego, 1986.

Jenkins, J. T., and D. M. Hanes, A sheared layer of colliding grains driven from above by a turbulent fluid, *J. Fluid Mech.*, *370*, 29–52, 1998.

Jimenez, J. A., A. Sánchez-Arcilla, and G. Rodriguez, Sediment resuspension under non-breaking waves: Predicting sediment "pulses" as a function of groupiness, in *Proc. of the 26th Int. Conf. on Coast. Eng., Copenhagen, Denmark*, pp. 2595–2606, Am. Soc. of Civ. Eng., Reston, Va., 1998.

Jonsson, I. G., Wave boundary layers and friction factors, in *Proc. 10th Int. Conf. on Coast. Eng.*, pp. 127–148, Am. Soc. of Civ. Eng., Reston, Va., 1966.

King, D. B., Studies in oscillatory flow bedload sediment transport, Ph.D. Thesis, Univ. of Calif., San Diego, 1991.

Kroon, A., Sediment transport and morphodynamics of the beach and nearshore zone near Egmond, The Netherlands, Ph.D. Thesis, 275 pp., Univ. of Utrecht, Utrecht, 1994.

Lee, T. H., and D. M. Hanes, Comparison of field observations of the vertical distribution of suspended sand and its prediction by models, *J. Geophys. Res.*, *101*, 3561–3572, 1996.

Li, L., and M. Sawamoto, Experiments on sediment transport in sheet-flow regime under oscillatory flow, *Coast. Eng. Jpn.*, *38*(2), 143–156, 1995.

Lohrmann, A., R. Cabrera, and N. C. Kraus, Acoustic-Doppler Velocimeter (ADV) for laboratory use, in *Proc. Symp. on Fundam. and Adv. in Hydraul. Meas. and Exp., 1–5 August, Buffalo, N. Y.*, Am. Soc. of Civ. Eng., Reston, Va., pp 351–365, 1994.

McLean, S. R., J. S. Ribberink, C. M. Dohmen-Janssen, and W. N. Hassan, Sand transport in oscillatory sheet flow with mean current, *J. Waterw. Port Coast. Ocean Eng., ASCE*, *127*(3), 141–151, 2001.

Ribberink, J. S., Bed-load transport for steady flows and unsteady oscillatory flows, *Coast. Eng.*, *34*, 59–82, 1998.

Ribberink, J. S., and A. A. Al-Salem, Sediment transport in oscillatory boundary layers in cases of rippled bed and sheet-flow, *J. Geophys. Res.*, *99*, 12,707–12,727, 1994.

Ribberink, J. S., and A. A. Al-Salem, Sheet flow and suspension in oscillatory boundary layers, *Coast. Eng.*, *25*, 205–225, 1995.

Ribberink, J. S., C. M. Dohmen-Janssen, D. M. Hanes, S. R. McLean, and C. E. Vincent, Near-bed sand transport mechanisms under waves: A large-scale flume experiment (SISTEX99), in *Proc. of the 27th Int. Conf. on Coast. Eng. 2000, Sydney*, pp. 3263–3276, Am. Soc. of Civ. Eng., Reston, Va., 2000.

Sawamoto, M., and T. Yamashita, Sediment transport rate due to wave action, *J. Hydrosci. Hydraul. Eng.*, *4*(1), 1–15, 1986.

Smith, J. D., Modeling of sediment transport on continental shelves, in *The Sea,* Vol. 6, pp. 539–577, Wiley-Interscience, New York, 1977.

Sumer, B. M., A. Kozakiewicz, J. Fredsøe, and R. Deigaard, Velocity and concentration profiles in sheet-flow layer of movable bed, *J. Hydrol. Eng., ASCE*, *122*(10), 549–558, 1996.

Swart, D. H., Offshore sediment transport and equilibrium beach profiles, *Delft Hydraul. Lab., Publ. 131*, Delft Hydraul., The Netherlands, 1974.

Thorne, P. D., and D. M. Hanes, A review of acoustic methods for the study of small scale sediment transport processes, *Cont. Shelf Res.*, *22*, 603–632, 2002.

Van der Hout, G., Grain size and gradation effects on sediment transport under sheet flow conditions, *Report Z2137, Part II, October 1997*, Delft Hydraul., The Netherlands, 1997.

Van Rijn, L. C., The effect of sediment composition on cross-shore bed profiles, in *Proc. of the 26th Int. Conf. on Coast. Eng., Copenhagen, Denmark*, pp. 2495–2508, Am. Soc. of Civ. Eng., Reston. Va., 1998.

Vincent, C. E., and M. O. Green, Field measurements of the suspended sand concentration profiles and fluxes and of the resuspension coefficient γ_0 over a ripple bed, *J. Geophys. Res.*, *95*, 11,591–11,601, 1990.

Wilson, K. C., Mobile bed friction at high shear stress, *J. Hydrol. Eng., ASCE*, *115*(6), 825–830, 1989.

Zala Flores, N., and J. F. A. Sleath, Mobile layer in oscillatory sheet flow, *J. Geophys. Res.*, *103*, 12,783–12,793, 1998.

C. M. Dohmen-Janssen, Department of Civil Engineering, University of Twente, PO Box 217, 7500 AE, Enschede, Netherlands, (c.m.dohmen-janssen@ctw.utwente.nl)

D. M. Hanes, Department of Civil and Coastal Engineering, University of Florida, Gainesville, FL 32611-6590, USA. (hanes@ufl.edu)